

# Prognostication of Helicopter Failure

**November 2009**

Prepared by  
L. M. Hively, Ph.D.  
Oak Ridge National Laboratory

#### DOCUMENT AVAILABILITY

Reports produced after January 1, 1996, are generally available free via the U.S. Department of Energy (DOE) Information Bridge:

**Web site:** <http://www.osti.gov/bridge>

Reports produced before January 1, 1996, may be purchased by members of the public from the following source:

National Technical Information Service  
5285 Port Royal Road  
Springfield, VA 22161  
**Telephone:** 703-605-6000 (1-800-553-6847)  
**TDD:** 703-487-4639  
**Fax:** 703-605-6900  
**E-Mail:** [info@ntis.fedworld.gov](mailto:info@ntis.fedworld.gov)  
**Web site:** <http://www.ntis.gov/support/ordernowabout.htm>

Reports are available to DOE employees, DOE contractors, Energy Technology Data Exchange (ETDE) representatives, and International Nuclear Information System (INIS) representatives from the following source:

Office of Scientific and Technical Information  
P.O. Box 62  
Oak Ridge, TN 37831  
**Telephone:** 865-576-8401  
**Fax:** 865-576-5728  
**E-mail:** [reports@adonis.osti.gov](mailto:reports@adonis.osti.gov)  
**Web site:** <http://www.osti.gov/contact.html>

This report was prepared as an account of work sponsored by an agency of the United States Government. Neither the United States government nor any agency thereof, nor any of their employees, makes any warranty, express or implied, or assumes any legal liability or responsibility for the accuracy, completeness, or usefulness of any information, apparatus, product, or process disclosed, or represents that its use would not infringe privately owned rights. Reference herein to any specific commercial product, process, or service by trade name, trademark, manufacturer, or otherwise, does not necessarily constitute or imply its endorsement, recommendation, or favoring by the United States Government or any agency thereof. The views and opinions of authors expressed herein do not necessarily state or reflect those of the United States Government or any agency thereof.

**PROGNOSTICATION OF HELICOPTER GEAR FAILURE**

L. M. Hively, Ph.D.  
Oak Ridge National Laboratory

Date Published: November 2009

Prepared by  
OAK RIDGE NATIONAL LABORATORY  
P.O. Box 2008  
Oak Ridge, Tennessee 37831-6285  
Managed by  
UT-Battelle, LLC  
for the  
U.S. DEPARTMENT OF ENERGY  
under contract DE-AC05-00OR22725



## TABLE OF CONTENTS

Section Title	Page
TABLE OF CONTENTS .....	iii
LIST OF FIGURES.....	v
LIST OF TABLES .....	vii
ACKNOWLEDGMENTS.....	ix
ABSTRACT.....	1
1. INTRODUCTION .....	3
2. BACKGROUND .....	5
3. ANALYSIS METHODOLOGY.....	6
4. RESULTS .....	10
5. CONCLUSIONS .....	15
6. REFERENCES .....	17



## LIST OF FIGURES

<b>Figure</b>	<b>Page</b>
Figure 1. US Army's OH-580C helicopter. ....	23
Figure 2. Pictures of the OH-58C gearbox .....	24
Figure 3. Spiral-bevel pinion gear from OH-58C helicopter before removal of the broken tooth. ....	25
Figure 4. Typical data from the OH-58C helicopter gearbox experiment. ....	26
Figure 5. Typical measures of data from the OH-58C helicopter gearbox experiment .....	28
Figure 6. Typical measures of data from OH-58C helicopter gearbox experiment. ....	29
Figure 7. Typical measures of data from OH-58C helicopter gearbox experiment .....	30
Figure 8. Typical measures of data from OH-58C helicopter gearbox experiment. ....	31
Figure 9. Typical measures of data from OH-58C helicopter gearbox experiment .....	32
Figure 10. Traditional nonlinear measures of the first accelerometer channel. ....	33
Figure 11. Traditional nonlinear measures of the second accelerometer channel. ....	34
Figure 12. Traditional nonlinear measures of the third accelerometer channel .....	35
Figure 13. Traditional nonlinear measures of the fourth accelerometer channel .....	36
Figure 14. Traditional nonlinear measures of the fifth accelerometer channel. ....	37
Figure 15. Phase-space dissimilarity measures versus time for accelerometer channel. ....	38
Figure 16. Best forewarning of gear failure via the composite phase-space dissimilarity measure .....	39
Figure 17. Best forewarning of gear failure via the composite phase-space dissimilarity measure .....	40
Figure 18. Best forewarning of gear failure via the composite phase-space dissimilarity measure .....	41
Figure 19. Best forewarning of gear failure via the composite phase-space dissimilarity measure. ....	42



## LIST OF TABLES

<b>Table</b>	<b>Page</b>
Table 1. Summary of Forewarning Criteria for Each Channel via Phase-Space Dissimilarity .....	12
Table 2. Summary of Measures for Each Channel .....	13
Table 3. Summary of Recent Machine Failure Forewarning Results .....	15



## **ACKNOWLEDGMENTS**

This work was sponsored by the U.S. Army Research Laboratory (ARL) under work-for-others inter-agency agreement, Proposal #2374-S714-A1, “Specialized R&D Support for the RDECOM,” Task 3.2 (In Support of Technology Development, Demonstration, and Validation). Oak Ridge National Laboratory is managed for the U.S. Department of Energy by UT-Battelle, LLC, under Contract No. DE-AC05-00OR22725. We thank ARL for providing the data that were analyzed here.



## **ABSTRACT**

The U.S. Army needs prognostic analysis of mission-critical equipment to enable condition-based maintenance before failure. ORNL has developed and patented prognostic technology that quantifies condition change from noisy, multi-channel, time-serial data. This report describes an application of ORNL's prognostic technology to failure forewarning for the main-rotor gearbox of the Army's OH-58C Kiowa (Bell 206B) helicopter. The first objective of this work was identification of easily-acquired, process-indicative data, namely accelerometer data. The second objective of this work was avoidance of the garbage-in-garbage-out syndrome via data quality analysis, which did not identify any problems with the accelerometer data. The third objective was condition-change analysis to forewarn of a seeded fault in the spiral-bevel pinion gear. ORNL's phase-space dissimilarity approach provides forewarning of the gear failure from the accelerometer data. We conclude that ORNL's technology is an excellent candidate to meet the U.S. Army's need for prognostication.



## 1. INTRODUCTION

Real-time prognostication of mission-critical equipment is required to avoid unexpected failures. Typical failures include structural cracking, misalignment, imbalance, short-circuit, broken gears, bearing faults, dust clogging, exhaust deposits on internal parts, and severe wear from wind-blown particulates. Recent information-technology developments (e.g., low-form-factor micro-processors; low-cost, wireless, reduced-size sensors; mesh networking) can now be combined with advanced-prognostics software for longer prediction horizons, while adding minimal weight and bulk.

ORNL staff have developed and patented a novel, advanced statistical method that detects condition change from noisy, multi-channel, time-serial data. ORNL has demonstrated the prognostic technology for both biomedical<sup>1-15</sup> and machine applications<sup>15-26</sup>. Specific machine demonstrations to date include both accelerated failure tests and seeded faults in motors and motor-driven components:

- Detection of progressively larger drill bit wear from spindle-motor current<sup>21</sup>;
- Distinction between different states for (un)balanced centrifugal pump from motor power<sup>21</sup>;
- Detection of progressively larger crack in rotating blade from vibration and electrical power<sup>22</sup>;
- Forewarning of gear failure from torque and vibration data<sup>22</sup>;
- Forewarning of bearing failure from vibration data<sup>22</sup>;
- Motor faults (air-gap offset, cut rotor, turn-to-turn short, imbalance) from power<sup>23</sup>;
- Imbalance and misalignment faults in a motor-driven pump from electrical power<sup>24</sup>;
- Forewarning of structural failure from stress and strain data<sup>18-20, 25</sup>.

The technology readiness level (TRL) is five, involving integrated, high-fidelity demonstration of the technology components for realistic environments.

The model-independent, data-driven approach quantifies dynamical change in nonlinear systems from time-windowed data sets. The method first rejects inadequate-quality data. Next, a novel filter removes confounding artifacts (e.g., fundamental sinusoid in electrical data). The artifact-filtered data then are converted to a discrete dynamical signature in the form of a statistical distribution function (DF) via time-delay phase-space reconstruction. Dissimilarity measures quantify condition change between the baseline (normal state) DF and subsequent test case DFs. Several sequential occurrences of the dissimilarity measures above a threshold indicate significant change, as a forewarning of failure. This approach also provides an indication of failure onset. This approach has been demonstrated for motors and motor-driven components over more than three orders of magnitude in power (0.25 to 800-HP). PDF copies of our reports<sup>1-26</sup> and patents<sup>27-34</sup> are available at the author's publications link, [http://computing.ornl.gov/cse\\_home/staff/hively.shtml](http://computing.ornl.gov/cse_home/staff/hively.shtml).

The objectives of this work are: (1) identification of easily-acquired, process-indicative data for the machine's health status; (2) data quality analysis to avoid the garbage-in-garbage-out syndrome; (3) condition-change analysis to indicate operational stress under non-ideal operation and machine degradation in proportion to the operational stress or degradation; and (4) forewarning of failure if it occurs. The long-term goal is determination of the remaining useful operational life, or equivalently an estimate for the time to failure. This report is organized as follows. Section 2 provides background information for the work. Section 3 describes the analysis methodology. Section 4 discusses the results. Section 5 presents the conclusions.



## 2. BACKGROUND

Reliable prognostication is very difficult. The major roadblocks include<sup>35-37</sup>: (a) an incomplete understanding of fault evolution and failure physics (e.g., different degradation rates for various machine components); (b) the lack of predictive methodologies for unsteady failure signatures; (c) the need for up-to-date trends in component condition and life span; (d) ignorance about controlling parameters (e.g., initial condition, service environment, and maintenance history); (e) emulation of a real operating environment. Previous ORNL work<sup>16</sup> provided a brief history of dynamical machine analysis over the last 40 years, which will not be repeated here. Our present approach addresses items (a)-(c) by quantifying the (non-stationary) condition change as a sequence of nonlinear statistical signatures from process-indicative data; item (d) by associating change in the controlling parameter with the dynamical signature of the equipment response; and item (e) by acquisition and analysis of test data that are similar to real-life operations.

Condition-based maintenance<sup>37</sup> enhances reliability and operational readiness by indicating the equipment's present state (diagnostic), as well as estimating its future condition (prognostic). The advantages of condition-based maintenance include: increase in availability; reduction in downtime; reduction in mission aborts arising from equipment failure; improvement in management and planning of maintenance; lower total maintenance cost; verification of equipment condition prior to deployment; identification of repair/replacement needs before failure; reduction in needs for additional diagnostic equipment; and greater safety. The bottom line is higher mission success rate at lower cost in terms of lives, equipment, and dollars.

The present application is forewarning of helicopter gear failure. Frequent failures occur in the main-rotor gearbox. The sponsor provided failure-test data on a gearbox from the OH-58C Kiowa (Bell 206B) helicopter (maximum gross weight of 4,000 pounds), which is typically used for scouting missions (Figure 1). This report discusses failure prognostication of the spiral-bevel pinion gear in the OH-58C gearbox (Figure 2) via accelerated testing after introduction of a seeded fault (Figure 3).

### 3. ANALYSIS METHODOLOGY

For the reader's convenience, we summarize the analysis methodology<sup>15-16</sup>, utilizing three basic approaches, namely conventional statistical measures, traditional nonlinear measures, and ORNL's novel phase-space dissimilarity measures. A process-indicative scalar signal,  $e$ , is sampled at equal time intervals,  $\tau$ , starting at an initial time,  $t_0$ , yielding a time-serial sequence of  $N$  points,  $e_i = e(t_0 + i\tau)$ . Artifacts are removed from this data with a zero-phase quadratic filter<sup>34</sup> that performs better than conventional filters. This filter uses a moving window, with the same number of data points,  $w$ , on either side of a central point. A parabola is fitted in the least-squares sense over this window of  $2w+1$  data points. The central point of the fit is an estimate the low-frequency artifact,  $f_i$ . The residual (artifact-filtered) signal,  $g_i = e_i - f_i$ , has essentially no low-frequency artifact activity. All subsequent analysis uses this artifact-filtered data,  $g_i$ .

Conventional statistical measures<sup>38</sup> (CSM) provide a general characterization of data. Typical CSM are the mean:  $\bar{g} = \sum_i g_i/N$  (the sum over  $i$ ,  $\sum_i$ , includes  $N$  points in the analysis window); the absolute average deviation,  $a = \sum_i |g_i - \bar{g}|/N$ ; the sample standard deviation,  $\sigma = [\sum_i (g_i - \bar{g})^2/(N-1)]^{1/2}$ ; and the minimum,  $g_n$ , and maximum,  $g_x$ , in the signal. Higher moments are skewness (third moment):  $SK = \sum_i (g_i - \bar{g})^3/N\sigma^3$ , and kurtosis (fourth moment),  $KT = \sum_i (g_i - \bar{g})^4/N\sigma^4 - 3$ . Time-scale measures include the average number of time steps per cycle:  $m = N/[(n_c - 1)/2] \approx 2N/n_c$ , for  $n_c \gg 1$  ( $n_c =$  average number of crossings of the mean); and the first zero,  $Z$ , in autocorrelation function, which is defined as:  $A(j) = \sum_i (g_i - \bar{g})(g_{i+j} - \bar{g})/(N-j)\sigma^2$ . CSM are useful in the analysis of linear processes, but typically provide inconsistent discrimination of condition change in nonlinear systems. They are included here for completeness and comparison.

Traditional nonlinear measures (TNM) can be useful for characterization of nonlinear data. One is the maximum-likelihood correlation dimension<sup>39-40</sup>,  $D = -M\{\sum_{ij} \ln[(\delta_{ij}/\delta_0 - \delta_n/\delta_0)/(1 - \delta_n/\delta_0)]\}^{-1}$ , which measures complexity. Here,  $M$  is the number of randomly-sampled pairs of phase-space (PS) points. The distance between PS-point pairs,  $i$  and  $j$ , is  $\delta_{ij} = \max(0 \leq k \leq m-1) |g_{i+k} - g_{j+k}|$ , where  $m$  is the average number of data points per cycle, as defined above. The distance  $\delta_n$  is the scale length that is associated with noise. Distances are normalized with respect to a nominal scale length,  $\delta_0$ , which is a balance between sensitivity to local dynamics (typically at  $\delta_0 \leq \square 5a$ ) and avoidance of excessive noise (typically at  $\delta_0 \geq a$ ). Here, the symbol,  $a$ , denotes the absolute average deviation (defined in the paragraph on CSM) as a robust indicator of variability<sup>41</sup>.

Another typical TNM is Kolmogorov entropy (K-entropy),  $K$ , which measures the rate of information loss per unit time (e.g., bits per second as a measure of predictability), and is the sum of the positive Lyapunov exponents. Positive, finite  $K$  is generally viewed as an indication of chaotic dynamics. Very large entropy indicates a stochastic (totally unpredictable) phenomenon.  $K$  is estimated from the average number of time steps,  $b_i$ , for two PS points, initially within  $\delta \leq \delta_0$ , to diverge to  $\delta > \delta_0$ . The maximum-likelihood form of Schouten *et al.*<sup>41</sup> is  $K = -f_s \log(1 - 1/\underline{b})$ , with  $\underline{b} = \sum_i b_i/M$  for  $M$  point pairs. The data-sampling rate is  $f_s$ .

A third TNM is the mutual information function (MIF), which measures average bits of information that can be inferred from one measurement about a second, as a function of the time delay between the two signals. Shannon and Weaver<sup>42</sup> developed the MIF, which was later applied to time series<sup>43</sup>. The first minimum in the MIF,  $M_1$ , gives the average de-correlation time. The MIF is:  $I(q,r) = I(r,q) = H(q) + H(r) - H(r,q)$ . Here,  $H$  is the entropy:  $H(q) = -\sum_i P(q_i) \log_2[P(q_i)]$  and  $H(q,r) = -\sum_{ij} P(q_i, r_j) \log_2[P(q_i, r_j)]$ . One set of measurements is denoted by  $Q = \{q_1, q_2, \dots, q_N\}$ , with associated occurrence probabilities,  $P(q_1), P(q_2), \dots, P(q_N)$ . A second measurement set is  $R = \{r_1, r_2, \dots, r_N\}$ , with a time delay relative to  $Q$ , and with occurrence probabilities  $P(r_1), P(r_2), \dots, P(r_N)$ .  $P(q_i, r_j)$  is the joint probability that both states occur simultaneously. TNM usually do a poor job of discriminating condition change, but are also included for comparison and completeness.

The  $g_i$ -data are converted into  $S$  discrete (symbolized) values<sup>16</sup>,  $s_i$ , namely  $0 \leq s_i \leq S - 1$ . Equiprobable symbols are formed by ordering all  $N$  of the base case artifact-filtered, time-serial data points from the smallest to largest value. The first  $N/S$  of these ordered values correspond to the first symbol, 0. Ordered data values  $(N/S) + 1$  through  $2N/S$  correspond to the second symbol, 1, and so on. Equiprobable symbols have non-uniform partitions in the signal amplitude with the same occurrence frequency of  $g_i$  values by construction, and thus have no information about the dynamical structure. In contrast, symbols with uniform partitions (uniform symbols),  $s_i = S (g_i - g_n)/(g_x - g_n)$ , have inherent dynamical structure before beginning the PS reconstruction, where  $g_x$  and  $g_n$  are the maximum and minimum values of the  $g_i$ -data, respectively. Thus, one advantage of equiprobable symbols is that dynamical structure arises *only* from the PS reconstruction, as described below. Moreover, large negative and large positive values of  $g_i$  have little effect on equiprobable symbolization, but dramatically change the partitions for uniform symbols. The variable,  $UE$ , designates uniform ( $UE = 0$ ) or equiprobable ( $UE = 1$ ) symbols.

The time-serial  $s_i$ -data are next converted into a geometric object via phase-space (PS) reconstruction via time-delay vectors,  $y(i) = [s_i, s_{i+\mu}, \dots, s_{i+(d-1)\mu}]$ , partitioning the PS into  $S^d$  hypercubes or bins<sup>16</sup>. Each bin can be identified by a unique integer,  $J$ , via base- $S$  arithmetic,  $J = \sum_m s_{i+m\mu} S^m$ , where the summation,  $\sum_m$ , is over the range  $0 \leq m \leq d-1$ . Additional data channels may add more information about the inter-connected dynamics, implying that a multi-channel PS-vector could contain more information than a single channel. The multi-channel PS vector is:  $y(i) = [s_i(1), s_{i+\mu}(1), \dots, s_{i+(d-1)\mu}(1), \dots, s_i(C), s_{i+\mu}(C), \dots, s_{i+(d-1)\mu}(C)]$ . Here, the symbol,  $s(k)$  denotes values from the  $k$ -th channel,  $1 \leq k \leq C$ , for up to  $C$  channels. Now, the symbolization divides the multi-channel PS in  $S^{Cd}$  bins, where the bin identifier is  $J = \sum_k \sum_m s(k)_{i+m\mu} S^{m+d(k-1)}$ . The parameter choice determines how well the PS reconstruction characterizes the dynamics. For example, an excessively large embedding dimension could result in over-fitting of real data with finite length and noise. Moreover, different observables of a system contain unequal amounts of dynamical information, implying that PS reconstruction could be easier from one choice of variable(s), but more difficult or impossible from another choice. This analysis seeks to balance these caveats for finite-length noisy data.

Conversion of the time-serial data into discrete PS states allows the construction of a statistical distribution function (DF) by counting the number of PS points that occur in each bin<sup>16</sup>. This DF is the discretized density of PS states.  $Q_J$  and  $R_J$  denote the population of the  $J$ -th DF bin for the base case (nominal state), and for a test case (test state), respectively. The test case is compared to the base case by dissimilarity measures, namely the  $\chi^2$  statistic and  $L_1$  distance:

$$\chi_N^2 = \sum_J (Q_J - R_J)^2 / (Q_J + R_J), \quad (1)$$

$$L_N = \sum_J |Q_J - R_J|. \quad (2)$$

The sum in Eqs. (1) - (2) is over all of the populated PS bins. In this work,  $\chi_N^2$  is not an unbiased statistic for testing a null statistical hypothesis but rather is a *relative* measure<sup>7</sup> of dissimilarity between the two DFs. The  $L_1$  distance is the natural metric for DFs by its direct relation to the total invariant measure on the attractor. These measures account for changes in the geometry and visitation frequency of the attractor. Consistent calculation requires the same number of points in both the base and test case DFs, identically sampled; otherwise the distribution functions must be rescaled.

The accuracy and sensitivity of the PS reconstruction can be enhanced by connecting successive PS points as prescribed by the underlying dynamics,  $y(i) \rightarrow y(i+1)$ . A discrete representation of the process flow is formed by adjoining two successive vectors from the  $d$ -dimensional reconstructed PS,  $Y(i) = [y(i), y(i+1)]$ .  $Y(i)$  is a  $2d$ -dimensional, connected-phase-space (CPS) vector. As before,  $Q$  and  $R$  denote the CPS DFs for the base case and test case, respectively. The measures of dissimilarity between these two CPS DFs are defined via the  $L_1$ -distance and  $\chi^2$  statistic, as before:

$$\chi_C^2 = \sum_{JK} (Q_{JK} - R_{JK})^2 / (Q_{JK} + R_{JK}), \quad (3)$$

$$L_C = \sum_{JK} |Q_{JK} - R_{JK}|. \quad (4)$$

The subscript,  $C$ , denotes CPS measures in Eqs. (3) - (4), while the subscript,  $N$ , in Eqs. (1) - (2) denotes non-connected PS states. The subscripts,  $J$  and  $K$ , are identifiers for the initial,  $y(i)$ , and final,  $y(i+1)$ , PS states, respectively. The value  $\mu = 1$  results in  $d - 1$  components of  $y(i + 1)$  being redundant with those of  $y(i)$ ; this redundancy is allowed to accommodate other data such as discrete points from two-dimensional maps. CPS measures have higher discriminating power than their non-connected counterparts. Indeed, these measures rigorously satisfy the inequalities<sup>6</sup>:  $\chi_N^2 \leq L_N$ ,  $\chi_C^2 \leq L_C$ ,  $L_N \leq L_C$ , and  $\chi_N^2 \leq \chi_C^2$ .

The quantities in Eqs. (1) – (4) are called phase space dissimilarity measures (PSDM). These measures discriminate between different chaotic regimes, and transitions between regular and chaotic regimes. Such discrimination is impossible with traditional nonlinear measures (e.g., Lyapunov exponents, Kolmogorov entropy, correlation dimension<sup>44</sup>). Straightforward methods exist<sup>45-47</sup> for discriminating between regular and chaotic dynamics, or for detecting the transition between these regimes. The reason for this improvement is rather simple: discrimination by TNM is based on a difference of averages, while discrimination via PSDM is based on summing the absolute value of differences.

The disparate range and variability of these measures are difficult to interpret, especially for noisy data. A consistent means of comparison is via normalized dissimilarity measures (NDM)<sup>5-6</sup>, which are defined by the following form:  $U(V) = |V_i - \bar{V}| / \sigma_1$ , as the number of standard deviations,  $\sigma_1$ , that the test case deviates from the base case mean. The base case corresponds to the nominal-state dynamics.  $V$  denotes a phase-space dissimilarity measure from the set,  $V = \{L_N, L_C, \chi_N^2, \text{ and } \chi_C^2\}$ . We obtain the mean value,  $\bar{V}$ , of the dissimilarity measure by comparison among the  $B(B-1)/2$  unique combinations of the  $B$  base case cutsets, with a corresponding sample standard deviation,  $\sigma_1$ . We subsequently compare each contiguous, non-overlapping test case cutset to each of the  $B$  base case cutsets, and obtain the corresponding average dissimilarity value,  $V_i$ , of the  $i$ -th analysis window for each dissimilarity measure. A statistically significant trend in the NDM indicates equipment degradation for failure forewarning.

Our previous work<sup>4, 21-24</sup> found that the NDM are sensitive measures of condition change, but that further improvements are needed for an explicit indication of failure. A specific measure for end-of-life forewarning<sup>16</sup> is the sum of the four PSDM. The results of Section 4 illustrate that this composite,  $C_i$  for the  $i$ -th cutset, displays the same trends as the individual PSDM and is more robust than any one of the PSDM alone.

$$C_i = U(\chi_N^2) + U(\chi_C^2) + U(L_N) + U(L_C). \quad (5)$$

The best analysis parameters,  $\{N, w, B, S, d, \mu, UE\}$ , depend not only on the system, but also on the specific data under consideration. From experience, the longest analysis window of  $N$  points is best, limited by the total length of each data record,  $N = 225,000$ , as explained below. The number of base case cutsets is  $B = 10$ , as a balance between a reasonably short quasi-stationary period of “normal” dynamics and a sufficiently long period for statistical significance. Figure 4 shows that the accelerometer signals have no artifact, and hence this feature of the analysis is not used. Our analysis over the remaining parameters,  $\{S, d, \mu, UE\}$ , proceeds as follows: (a) choose the parameter set; (b) compute the normalized PS dissimilarity measures for the specific machine data; and (c) exhaustively search over the parameters for the best indication of condition change. More specifically, the analysis searches over the phase-space parameters for the earliest forewarning time.



#### 4. RESULTS FOR THE HELICOPTER-GEAR FAILURE

A series of experiments<sup>48-60</sup> were performed to predict failures in the OH-58C Kiowa helicopter (Figure 1), which the Army has used since 1969. The specific failure involved the main-rotor gearbox (Figure 2) with a maximum input torque of 350 N-m (3100 in-lb), a maximum input speed of 6060 RPM, and a net reduction ratio of 17.44:1. Tests used a test stand at the NASA-Glenn Research Center in Cleveland, Ohio.

The specific gear under study<sup>53-54</sup> is a 19-tooth spiral-bevel pinion that is driven directly by the input shaft to the gearbox. This pinion gear meshes with a 71-tooth ring gear in the first reduction stage. A seeded fault (notch) was formed by electro-discharge machining in the fillet region of one tooth of the spiral-bevel pinion (top of Figure 3) in order to initiate failure cracking. The gearbox was run at 1.5-times the maximum design torque and at maximum input speed to accelerate the failure of this seeded fault. The experimental diagnostics indicated failure onset after 4.15 hours at this torque overload. A 60X-microscopic visual inspection found no crack at 4.41 hours. The proximity probe data showed a once-per-revolution spike at 4.4723 hours, which was roughly 9 minutes before complete tooth separation from the gear at 4.621 hours (bottom of Figure 3).

The experimental diagnostics included five accelerometers (A1 – A5). Figure 2 shows the locations of these sensors. The present analysis uses the raw accelerometer data, as discussed in Sec. 3. These data<sup>53-54</sup> were sampled at 150 kHz with 12-bit precision for 1.5 seconds (225,000 points in each of 8 channels) during successive, contiguous, non-overlapping 15-second intervals. Each data record was saved to a separate, uniquely-named file (EPI $n$ .DAT) in binary format. Here,  $n$  is the file sequence number, which ranged from 0001 to 1008 prior to the 60X-visual examination, and from 0001 to 0039 after the visual examination, for a total of 1047 usable records over a total test-data length of 4.3635 hours. The data were extracted from the binary files and concatenated into a single dataset for this analysis. Figure 4 shows the complex, nonlinear dynamical signatures from the five accelerometers (rows) with successively greater resolution in time (columns from left to right). The Fourier spectra (right-most column of Figure 4) have broad high-frequency tails with no dominant frequency, which is characteristic of complex, nonlinear data.

Data quality analysis verifies important features in the data: proper number of data points; any intervals with unchanged amplitude; saturation at high or low limits as an indicator of improper data scaling; consistent amplitude across datasets in the test sequence; adequate sampling rate; excessive periodic content; and excessive noise. An adequate sampling rate should span the de-correlation time with a sufficient number of time samples. The de-correlation-time measures are the first minimum in the mutual information function ( $\geq 4$  time steps) and the first zero in the auto-correlation function ( $\geq 4$  time steps). Excessive periodicity obscures the underlying nonlinear dynamics and has more than 50% of the total area under the two largest peaks in the Fourier spectrum versus frequency. Excessive noise obliterates the useful information with disorderly signal values. Consequently, a measure of order in the signal (Shannon entropy,  $E$ ) versus the number of uniform data symbols ( $S$ ) allows determination of the average number of bits of information ( $b$ ) in the data as the maximum in  $E$  versus  $S = 2^b$ ; less than five bits of information corresponds to excessive noise. The garbage-in-garbage-out syndrome is avoided by rejection of data that fails one or more of these tests. This quality check did not indicate any problems with the five accelerometer channels, which are the focus of this analysis.

Accelerometers A1 and A2 were co-located on the gearbox, and acquired data in the transverse (X) and vertical (Z) directions (Figure 2). Axial acceleration (Y direction) was not obtained at this same location. Axial acceleration can only be inferred from accelerometers A3 – A4 for analysis of 3-dimensional vibration power. The gearbox housing is made of a magnesium alloy, which is not a particularly rigid material, and allows transmission of vibrations from one accelerometer location to another. These confounding effects are confirmed by careful comparison of the data from accelerometers A3 and A4 (Figure 4), which clearly have very different dynamical signatures. This comparison allows for a sound propagation (4940 m/s) across the gearbox (diameter  $\sim 1$  m), giving a time delay between A3 and A4 of 0.2ms, or 30 time steps at a sampling rate of 150 kHz. Thus, the present data are inappropriate to form three-dimensional vibration power.

Decker and Lewicki<sup>54</sup> provide the following insights into the results from the five accelerometer channels. Accelerometers A1-A2 showed the spiral bevel harmonics as the dominant components; A4-A5 also had significant spiral bevel mesh frequency components. Accelerometer 3 obtained the highest level of vibration, involving the spiral bevel mesh and the planetary mesh. A2 provided the best response with motion sensitivity in the transverse (X) direction and a location closest to the bevel-pinion gear. A3 - A4 provided significant indication of damage, being motion-sensitive in the X-Y plane, but receiving attenuated signals due to their more distant location from the pinion mesh. A1 and A5 provided the least information, with indication of damage after the other accelerometers. A1 is the only accelerometer that is motion-sensitive in the vertical direction. A5 did not show a major effect, perhaps because it was mounted differently from the others on the top cover stud bracket. The use of various linear measures did not allow failure forewarning<sup>54</sup> in A1-A5.

The considerations of the previous two paragraphs leave two options for analysis of these data. One involves use of data from co-located sensors A1 (Z-direction) and A2 (X-direction) to obtain vibration power in the X-Z plane only. The second involves analysis of the accelerometer data from one (or more) of the individual five accelerometers, A1 – A5. However, different observables have unequal amounts of dynamical information<sup>38</sup>, implying that dynamical analysis could be easier from one variable, but more difficult or impossible from another. Consequently, the present work analyzes the uni-axial data from each of the five accelerometers.

Figure 5 shows linear statistical measures for the first accelerometer channel (A1). The top plot shows the maximum ( $g_x$ ) in red, the standard deviation ( $\sigma$ ) in green, the absolute average deviation, ( $a$ ) in blue, and the minimum ( $g_n$ ) in black. The minimum and maximum vary erratically around a nominal value, showing no forewarning of the failure and no indication of failure onset at the end of the data. The standard deviation and absolute average deviation vary slightly during the first two hours of the test, then are constant, and finally decrease slightly in the last fifteen minutes before failure. This last shift is not significant, because its variation is consistent with that of the first two hours. Consequently, these measures provide no forewarning and no indication of failure. The second plot from the top is skewness, which varies randomly from -0.065 to -0.05 for time <4.4 hours, then decreases systematically to <-0.08 as an indication of failure onset. The third plot from the top is kurtosis, which varies irregularly between -0.5 and -0.35 during the first 4.25 hours, and then rises abruptly to >-0.35 after 4.25 hours as an indication of failure onset. The second plot from the bottom shows the number of time steps per cycle ( $T_{CYC}$ ), which varies between 36 and 40 during the first 4.25 hours, then drops abruptly to <36 as an indication of failure onset. The bottom plot displays the number of time steps to reach the first zero ( $Z_I$ ) in the auto-correlation, which constant at 17 (with two spikes to 18) during the first 2.3 hours, and then varies erratically between 17 and 18 during the second half of the test. This latter increase in variability is neither a clear forewarning nor a clear indication of failure. The number of bits ( $b$ ) of precision in the data is a constant,  $b=9$ , for all times and all channels, and consequently is not shown. Figures 6 – 9 display analogous results for accelerometer channels, A2 – A5, respectively.

Figure 10 shows traditional nonlinear measures for the first accelerometer channel (A1). The top plot shows the first minimum in the mutual information function,  $M_1$ , with spikes between 17 and 18 time steps. The frequency of these spikes increases erratically to 4.25 hours.  $M_1$  is constant at 17 time steps from 4.25-4.45 hours, followed by more spikes. These features do not provide clear forewarning or indication of failure onset. The middle plot displays the correlation dimension,  $D$ , which varies erratically with no clear forewarning or indication of failure onset. The bottom plot illustrates the Kolmogorov entropy,  $K$ , which varies irregularly with no clear forewarning. The rise in  $K$  after 4.25 hours is irregular and has the same range as the preceding period, and consequently is not a clear indication of failure onset. Figures 11-14 show analogous traditional nonlinear measures for accelerometer channels, A2 – A5, respectively.

Figure 15 displays typical PSDM for accelerometer channel, A1. The top four subplots show the individual PSDM for  $\chi_N^2$ ,  $\chi_C^2$ ,  $L_N$ , and  $L_C$ . The bottom subplot shows the composite PSDM,  $C_i$ , with the same trends as each individual PSDM. Consequently, the forewarning analysis focuses on the composite measure,  $C_i$  which varies erratically about some nominal value. Failure forewarning corresponds to several successive values of this composite measure above a threshold, the determination of which is discussed next.

Figure 16 (top subplot) shows  $\sum_m C_m$ , which is the cumulative sum of the composite measure from the beginning of the test to the  $i$ -th analysis window. The cumulative sum increases roughly linearly over the initial testing time. Consequently, a straight line through the origin can be fitted in a least-squares sense to the cumulative sum. The middle subplot of Figure 16 shows the standard deviation (SD) between the straight-line fit and the cumulative sum. The step-function jumps in the SD arise from isolated spikes in  $C_i$  (blue curve in Figure 16 bottom) during the first 1.5 hours of the test. The spikes in  $C_i$  (and the resultant step-function jumps in the SD) are not statistically significant, and are ignored in the subsequent analysis. A minimum in SD occurs at 2.3 hours, as denoted by the red star (\*) in the middle subplot of Figure 16. The slope of this best-fit straight line corresponds to a threshold value,  $U_{FW}=2.7015$  (green horizontal line in Figure 16 bottom), which is also labeled at the bottom left of that subplot. The bottom subplot illustrates that most  $C_i$  values fall below this threshold before 2.43 hours, corresponding to nominal gearbox operation.

A determination of failure forewarning is also shown in Figure 16 (bottom), corresponding to  $C_i > U_{FW}$  after 2.43 hours. The number of successive values of  $C_i > U_{FW}$  after 2.43 hours is 464, which is shown inside the parentheses, next to  $U_{FW}=2.7015$  in the bottom subplot. Before 2.43 hours (specifically, between 2.3 and 2.425), the largest number of successive occurrences of  $C_i > U_{FW}$  is 31, as denoted by “(31)” just below that time segment in the bottom subplot. This false indication is excluded by requiring  $>31$  successive occurrences above the threshold. The forewarning criterion then is  $\geq 32$  successive occurrences of  $C_i > U_{FW}=2.7015$ ; the start of forewarning is at 2.56 hours (32 time windows after 2.43 hours at 15 seconds per time window).

Figure 16 (bottom) further displays the determination of failure onset. The smallest value of  $C_i$  during the failure onset period is  $U_{FAIL}=21.68$ ; the red horizontal line corresponds to this failure threshold. The value of  $C_i \geq U_{FAIL}$  occurs 40 times in succession. These two parameters are explicitly labeled as “ $U_{FAIL}=21.68(40)$ ” in the upper right of Figure 16 (bottom). Prior to failure onset only two values occur in succession above  $U_{FAIL}$ , as denoted by “(2)” near the peak at 0.6 hours. Consequently, the failure-onset criterion is  $\geq 3$  successive occurrences of  $C_i > U_{FAIL}=21.68$ . Analogous plots for accelerometer channels A2, A3, and A5 are displayed in Figures 17-19. Table 1 summarizes the results on the basis of the results in Figures 16–19. The analysis found no forewarning or failure onset in accelerometer channel A4, as denoted by, “--”, in the A4 column.

**Table 1. Summary of Forewarning Criteria for Each Channel via Phase-Space Dissimilarity**

Feature	Accelerometer Channel Designation				
	A1	A2	A3	A4	A5
Forewarning threshold, $U_{FW}$	2.7015	4.3122	2.7836	--	16.4579
Successive occurrences above $U_{FW}$	$\geq 32$	$\geq 52$	$\geq 13$	--	$\geq 64$
Threshold for failure onset, $U_{FAIL}$	21.68	27.425	1.2519	--	19.24
Successive occurrences above $U_{FAIL}$	$\geq 3$	$\geq 10$	$\geq 33$	--	$\geq 24$
Number of phase-space symbols, $S$	2	2	11	--	12
Dimension of phase space, $d$	3	3	3	--	3
Phase-space, time-delay lag, $\lambda$	30	10	12	--	20
Start of forewarning (hours)	2.56	2.58	4.29	--	4.18
Longest non-forewarning time (hours)	2.30 – 2.47	2.15 – 2.36	1.27 – 1.31	--	2.64 – 2.90
Start of failure indication (hours)	4.21	4.24	4.20	--	4.29

Table 2 summarizes the results versus accelerometer channel. The abbreviations are: no forewarning (NF), no indication of failure (NIF), indication of failure onset (IFO), and failure forewarning (FF). The last two are in bold font, consistent with the goal of this analysis. Kurtosis indicates failure onset in 4 channels (A1, A2, A4, and A5). Skewness indicates failure onset in 3 channels (A1 – A3). Two channels indicate failure onset via time steps per cycle (A1 – A2) and first zero in the autocorrelation (A2 – A3). First minimum in the mutual information indicates failure onset in one channel (A2). These weak indications are consistent with earlier work by Lewicki *et al.*<sup>53-54</sup>. The PSDM show forewarning and failure onset in 4 channels (A1, A2, A3, A5).

**Table 2. Summary of Measures for Each Channel**

Measure	Accelerometer Channel Designation				
	A1	A2	A3	A4	A5
Maximum	NF NIF	NF NIF	NF NIF	NF NIF	NF NIF
Minimum	NF NIF	NF NIF	NF NIF	NF NIF	NF NIF
Standard deviation	NF NIF	NF NIF	NF NIF	NF NIF	NF NIF
Absolute average deviation	NF NIF	NF NIF	NF NIF	NF NIF	NF NIF
Skewness	NF <b>IFO</b>	NF <b>IFO</b>	NF <b>IFO</b>	NF NIF	NF NIF
Kurtosis	NF <b>IFO</b>	NF <b>IFO</b>	NF NIF	NF <b>IFO</b>	NF <b>IFO</b>
Time steps per cycle	NF <b>IFO</b>	NF <b>IFO</b>	NF NIF	NF NIF	NF NIF
First zero in autocorrelation function	NF NIF	NF <b>IFO</b>	NF <b>IFO</b>	NF NIF	NF NIF
First minimum in mutual information	NF NIF	NF <b>IFO</b>	NF NIF	NF NIF	NF NIF
Correlation dimension	NF NIF	NF NIF	NF NIF	NF NIF	NF NIF
Kolmogorov entropy	NF NIF	NF NIF	NF NIF	NF NIF	NF NIF
Composite phase-space dissimilarity	<b>FF IFO</b>	<b>FF IFO</b>	<b>FF IFO</b>	NF NIF	<b>FF IFO</b>



## 5. CONCLUSIONS

This work analyzed accelerometer data from the Army’s OH-58C helicopter gearbox. The specific measures are conventional statistical measures (CSM), traditional nonlinear measures (TNM), and phase-space dissimilarity measures (PSDM). CSM are minimum, maximum, average, sample standard deviation, skewness, kurtosis, average time steps per cycle, and first zero in the auto-correlation function. The TNM include first minimum in the mutual information function as a measure of decorrelation time, correlation dimension as a measure of complexity, and Kolmogorov entropy as a measure of information loss rate. PSDM are the  $\chi^2$  statistic and  $L_1$  distance between the time-delayed reconstructions of the phase-space-distribution functions. The CSM and TNM provided weak indication of failure onset, and no failure forewarning. Specifically, kurtosis indicated failure onset in 4 channels (A1, A2, A4, and A5). Skewness indicated failure onset in 3 channels (A1 – A3). Two channels indicated failure onset via time steps per cycle (A1 – A2) and first zero in the autocorrelation (A2 – A3). First minimum in the mutual information indicated failure onset in one channel (A2). In sharp contrast to these weak indications, ORNL’s novel phase-space dissimilarity measures provided forewarning of the failure, as well as indication of the failure onset in four channels (A1, A2, A3, and A5).

Recent work by our team showed very similar results for other machines and types of data<sup>16</sup>. Namely, the PSDM provide a more consistent correlation with fault progression, than the CSM and TNM<sup>22</sup>. Table 3 summarizes recent results for forewarning of seeded faults and accelerated failures in a variety of equipment, along with multiple repetitions of the experiments for reproducibility.

**Table 3. Summary of recent machine failure forewarning results**

Provider	Equipment	Failure	Time-serial data	Reference
EPRI	800-HP electric motor	air-gap offset	electrical & vibration power	16, 23
EPRI	800-HP electric motor	broken rotor	electrical & vibration power	16, 23
EPRI	500-HP electric motor	turn-to-turn short	electrical & vibration power	16, 23
Otero	¼-HP electric motor	imbalance	Acceleration	23
PSU/ARL	30-HP motor	gear tooth	electrical & vibration power, torque	16, 23
PSU/ARL	motor	cracked blade	electrical & vibration power	16
PSU/ARL	30-HP motor	bearing	vibration power	16
ORNL	Dogbone samples	structural failure	stress & strain	18-20, 25
ORNL	Machine tool	chatter	Acceleration	26

PSDM consistently show better discrimination power for machine prognostication than either CSM or TNM. The reason for the improved performance of PSDM is that CSM and TNM compare averages, while PSDM are the sum over the absolute difference between the two phase-space states. In addition, the enhanced discrimination power facilitates use of PSDM on noisier data. The sensitivity and robustness of PSDM depend both on the data quality and on the phase-space reconstruction parameters. Indeed, (i) data quality can be improved by removal of confounding artifacts from the signal, and (ii) reconstruction parameters can be chosen much closer to their optimal values. In practice, the analysis requires a search over the parameter space to obtain the best indication of condition change.

*R&D Magazine* gave an R&D100 award to ORNL in 2005 for a hand-held prognostic device (SeizAlert<sup>10</sup>), which wirelessly acquires scalp brain waves, indicates forewarning of epileptic seizures, and provides the results wirelessly. Since ORNL has demonstrated that the same methodology works for both equipment and biomedical applications, this hand-held platform can be readily adapted for Army prognostics. We recommend the following implementation path for a failure- prognostication prototype: 1) acquisition of tri-axial accelerometer data from a single location on the helicopter gearbox for conversion to vibration power; 2) ten repetitions of the gear failure experiment for statistically defensible results; 3) implementation of the acquisition, analysis, and forewarning on a ruggedized, hand-held platform; and 4) prototype testing and validation in the field.



## REFERENCES

- <sup>1</sup> L. M. Hively, V. A. Protopopescu, N. B. Munro, "Enhancements in Epileptic Forewarning via Phase Space Dissimilarity," *J. Clin. Neurophysiol.* 22 (December 2005) 402-409.
- <sup>2</sup> L. M. Hively and V. A. Protopopescu, "Advanced Physiological Monitoring of FCS Soldiers," Proc. 24th Army Sci. Conf. (Orlando, FL) 29 Nov. – 2 Dec 2004.
- <sup>3</sup> L. M. Hively and V. A. Protopopescu, "Channel-Consistent Forewarning of Epileptic Events from Scalp EEG," *IEEE Trans. Biomed. Engr.* 50 (May 2003) 584-593.
- <sup>4</sup> L. M. Hively and V.A. Protopopescu, "Detection of Changing Dynamics in Physiological Time Series," *Proc. ANS Conf. on Nucl. Math. Computational Sci.* (Gatlinburg, Tn) 6-11 April 2003.
- <sup>5</sup> V. A. Protopopescu, L. M. Hively, P. C. Gailey "Epileptic Event Forewarning from Scalp EEG," invited review paper in *J. Clin. Neurophysiol.* 18 (May 2001) 223-245.
- <sup>6</sup> L.M. Hively, V.A. Protopopescu, P.C. Gailey, "Timely Detection of Dynamical Change in Scalp EEG Signals," *Chaos* 10 (2000) 864-875.
- <sup>7</sup> L.M. Hively, P.C. Gailey, and V.A. Protopopescu, "Detecting Dynamical Change in Nonlinear Time Series," *Physics Lett. A* 258 (1999) 103-114.
- <sup>8</sup> P.C. Gailey, L.M. Hively, V.A. Protopopescu, "Robust Detection of Dynamical Change in EEG," in *Proceedings of 5<sup>th</sup> Experimental Chaos Conference*, Orlando, Florida (6/28-7/1/99).
- <sup>9</sup> L.M. Hively, P.C. Gailey, V.A. Protopopescu, "Sensitive Measures of Condition Change in EEG Data," *Proc. of Int'l workshop Chaos in Brain* (Bonn, March 1999) World Scientific Publ.
- <sup>10</sup> L.M. Hively, K.L. Kruse, N.B. Munro, and V. A. Protopopescu, "Epilepsy Forewarning Using a Hand-Held Device," *ORNL/TM-2005/40* (February 2005) Oak Ridge National Laboratory, Oak Ridge, TN.
- <sup>11</sup> L. M. Hively, V. A. Protopopescu, J. Joseph, "CRADA Final Report for CRADA Number ORNL99-0559 – Epileptic Seizure Forewarning by Nonlinear Techniques," C/ORNL99-0559 (January 2002) Oak Ridge National Laboratory.
- <sup>12</sup> L.M. Hively, N.E. Clapp, V.A. Protopopescu, J. Joseph, C. E. Merican, T. Lucht, "Epileptic Seizure Forewarning by Nonlinear Techniques," *ORNL/TM-2000/333* (November 2000) Oak Ridge National Laboratory.
- <sup>13</sup> L.M. Hively, N.E. Clapp *Nonlinear Analysis of Polygraph Data, K/NSP-351* (March 1996) Oak Ridge National Laboratory, Oak Ridge, Tn.
- <sup>14</sup> L.M. Hively, N.E. Clapp, C.S. Daw, W.F. Lawkins, *Nonlinear Analysis of EEG For Epileptic Seizures*, ORNL/TM-12961 (April 1995) Oak Ridge National Laboratory.
- <sup>15</sup> V. Protopopescu and L.M. Hively, "Phase-space Dissimilarity Measures of Nonlinear Dynamics: Industrial and Biomedical Applications," *Recent Res. Devel. Physics* 6 (2005) 649-688.
- <sup>16</sup> L.M. Hively and V.A. Protopopescu, "Machine Failure Forewarning via Phase-Space Dissimilarity Measures," *Chaos* 14 (June 2004) 408-419.

- <sup>17</sup> V. A. Protopopescu, L. M. Hively, "Forewarning of Machine Failure via Nonlinear Analysis," *Proc. Amer. Nucl. Soc.*, June 2003.
- <sup>18</sup> D.E. Welch, L.M. Hively, R.F. Holdaway, "Nonlinear Crack Growth Monitoring", abstract for *33rd National Symp. On Fatigue and Fracture* (June 2001) Moran, Wyoming.
- <sup>19</sup> D.E. Welch, L.M. Hively, R.F. Holdaway, "Nonlinear Crack Growth Monitoring", *Proc. Int'l Mech. Engr. Congress and Exposition* (5-10 November 2000) Orlando, Florida.
- <sup>20</sup> D.E. Welch, L.M. Hively, R.F. Holdaway, "Nonlinear Crack Growth Monitoring", abstract accepted for *2000 ASM Materials Solutions Conference and Exposition* (11 October 2000) St. Louis, Missouri.
- <sup>21</sup> L.M. Hively, "Data-Driven Nonlinear Technique for Condition Monitoring," *Proc. Maintenance and Reliability Conf.*, Vol. 1, pp 16.01-16.10 (1997) Knoxville, Tn.
- <sup>22</sup> L. M. Hively, V. A. Protopopescu, K. M. Reichard, K. P. Maynard, "Nuclear Energy Research Initiative (NERI), Forewarning of Failure in Critical Equipment at Next-Generation Nuclear Power Plants," *ORNL/TM-2003/222*, October 23, 2003.
- <sup>23</sup> L. M. Hively and V. A. Protopopescu, "Forewarning of Failure in Critical Equipment at Next Generation NPP," Annual Report for NERI2000-109 project (Dec. 2002) *ORNL/TM-2002/183*.
- <sup>24</sup> L. M. Hively, V. A. Protopopescu, M. Maghraloui, and J. W. Spencer, "Annual Report for NERI Proposal #2000-0109 on Forewarning of Failure in Critical Equipment at Next-Generation Nuclear Power Plants," *ORNL/TM-2001/195* (November 2001).
- <sup>25</sup> D. E. Welch, L. M. Hively, R. F. Holdaway, "Nonlinear Crack Growth Monitoring," *ORNL-TM-1999/117*, October 1999.
- <sup>26</sup> L.M. Hively, V.A. Protopopescu, N.E. Clapp, C.S. Daw, Prospects of Chaos Control of Machine Tool Chatter, *ORNL/TM-13283* (June 1998).
- <sup>27</sup> L.M. Hively, "Methods for improved forewarning of critical events across multiple data channels," *U.S. Patent #7,209,861* (24 April 2007).
- <sup>28</sup> L.M. Hively, "Methods for consistent forewarning of critical events across multiple data channels," *U.S. Patent #7,139,677* (21 November 2006).
- <sup>29</sup> L.M. Hively, P.C. Gailey, V.A. Protopopescu, "Condition Assessment of Nonlinear Processes," *U.S. Patent #6,484,132* (19 November 2002).
- <sup>30</sup> D.E. Welch, L.M. Hively, and R.F. Holdaway, "Nonlinear Structural Crack Growth Monitoring," *U.S. Patent #6,460,012* (01 October 2002).
- <sup>31</sup> L.M. Hively, N.E. Clapp, C.S. Daw, W.F. Lawkins, "Epileptic Seizure Prediction By Non-linear Methods," *U.S. Patent #5,857,978* (12 January 1999).
- <sup>32</sup> L.M. Hively and E.G. Ng, "Integrated Method for Chaotic Time Series Analysis," *U.S. Patent #5,815,413* (29 September 1998).
- <sup>33</sup> L.M. Hively, N.E. Clapp, C.S. Daw, W.F. Lawkins, "Apparatus and Method for Epileptic Seizure Detection using Nonlinear Techniques," *U.S. Patent #5,743,860* (28 April 1998).

- <sup>34</sup> N.E. Clapp and L.M. Hively, "Method and Apparatus for Extraction of Low-Frequency Artifacts from Brain Waves for Alertness Detection," *U.S. Patent #5,626,145* (6 May 1997).
- <sup>35</sup> J.B. Andriulli, A.E. Gates, H.D. Haynes, L.B. Klett, S.N. Matthews, E.A. Nawrocki, P.J. Otaduy, M.B. Scudiere, T.J. Theiss, J.F. Thomas, L.M. Tolbert, M.L. Yaus, and C.A. Voltz, "Advanced Power Generation Systems for the 21<sup>st</sup> Century: Market Survey and Recommendations for A Design Philosophy," *ORNL/TM-1999/213* (Oak Ridge National Laboratory, Oak Ridge, TN) 1999.
- <sup>36</sup> J.B. Andriulli, M.B. Scudiere, C.P. White, G. Farquaharson, T.J. Theiss, C.W. Ayres, C.L. Coomer, D. Eddy, H.D. Ferguson, E.J. Hardin, H.D. Haynes, M.S. Hileman, D.K. Irick, L.B. Klett, P.J. Otaduy, G.W. Ott, W. Peterson, L.E. Sieber, J.F. Thomas, and L.M. Tolbert, "Development of Proof-of-Concept Units for the Advanced Medium-Sized Mobile Power Sources (AMMPS) Program," *ORNL/TM-2001/222* (Oak Ridge National Laboratory, Oak Ridge, TN) 2002.
- <sup>37</sup> *NIST Workshop on Condition-Based Maintenance*, [http://www.nist.gov/www/cbm/cbm\\_wp1.htm](http://www.nist.gov/www/cbm/cbm_wp1.htm).
- <sup>38</sup> M. Abramowitz and I.A. Stegun (ed.), *Handbook of Mathematical Functions*, U.S. Government Printing Office, Washington, D.C. (1964).
- <sup>39</sup> F. Takens, *Lecture Notes in Mathematics* 1125 (1984) 99–106.
- <sup>40</sup> J. C. Schouten, F. Takens, and C. M. van den Bleek, *Phys. Rev. E* 50 (1994) 1851-1861.
- <sup>41</sup> J. C. Schouten, F. Takens, and C. M. van den Bleek, *Phys. Rev. E* 49 (1994) 126-129.
- <sup>42</sup> C. E. Shannon and W. Weaver, *The Mathematical Theory of Communication* (Univ. of Illinois Press, Urbana, 1949).
- <sup>43</sup> A. M. Fraser and H. L. Swinney, *Phys. Rev. A* 33 (1986) 1134-40.
- <sup>44</sup> L. Qu, A. Xie and X. Li, "Study and performance evaluation of some nonlinear diagnostic methods for large rotating machines," *Mech. Mach. Theory* 28 (1993) 699-713.
- <sup>45</sup> J. P. Eckmann and D. Ruelle, *Rev. Mod. Phys.* 57 (1985) 617-655.
- <sup>46</sup> H. D. I. Abarbanel, *Analysis of Observed Chaotic Data* (Springer, New York) 1996.
- <sup>47</sup> A. Cover, J. Reneke, S. Lenhart, and V. Protopopescu, *Math. Models and Meth. in Appl. Sci.* 7 (1997) 823-845.
- <sup>48</sup> E.M. Huff, I.Y. Tumer, E. Barszcz, D.G. Lewicki, H.J. Decker, and J.J. Zakrajsek, "Experimental Analysis of Mast Lifting and Bending Forces on Vibration Patterns Before and After Pinion Reinstallation in an OH-58 Transmission Test Rig", *Proc. 56th American Helicopter Society International Forum* (Virginia Beach, VA) May 2000.
- <sup>49</sup> A.H. Pryor, M. Mosher, and D.G. Lewicki, "The Application of Time-Frequency Methods to HUMS", *Proc. 57th American Helicopter Society International Forum* (Washington, DC) May 2001.
- <sup>50</sup> H.J. Decker, "Gear Crack Detection Using Tooth Analysis", *56th Meeting of the Society for Machinery Failure Prevention Technology (MFPT)* (Virginia Beach, VA) 15-19 April 2002 (same as *NASA/TM-2002-211491* by NASA Glenn Research Center; Cleveland, OH and *ARL-TR-2681* by US Army Research Lab).

- <sup>51</sup> H.J. Decker, "Crack Detection for Aerospace Quality Spur Gears", *Proc. American Helicopter Society 58th Annual Forum* (Montreal, Quebec, Canada) 11-13 June 2002.
- <sup>52</sup> H.J. Decker, "Effects on Diagnostic Parameters after Removing Additional Synchronous Gear Meshes", *57th Meeting of the Society for Machinery Failure Prevention Technology (MFPT)* (Virginia Beach, VA) 14-18 April 2003 (same as *NASA/TM-2003-212312* by NASA Glenn Research Center; Cleveland, OH and *ARL-TR-2933* by US Army Research Lab).
- <sup>53</sup> H.J. Decker, and D.G. Lewicki, "Spiral Bevel Pinion Crack Detection in a Helicopter Gearbox", *Proc. 59th American Helicopter Society Annual Forum* (Phoenix, AZ) May 2003.
- <sup>54</sup> H.J. Decker and D.G. Lewicki, "Spiral Bevel Pinion Crack Detection in a Helicopter Gearbox," *NASA/TM-2003-212327* (NASA/Glenn Research Center, Cleveland, OH) and *ARL-TR-2958* (US Army Research Lab) June 2003.
- <sup>55</sup> H.J. Decker, and D.G. Lewicki, "Vibration Frequency Analysis Of A Helicopter Main Rotor Transmission During A Gear Crack Propagation Test", *Proc. 58th Meeting of the Society for Machinery Failure Prevention Technology (MFPT)* (Virginia Beach, VA) April 2004.
- <sup>56</sup> P.J. Dempsey, D.G. Lewicki, and H.J. Decker, "Investigation of Gear and Bearing Fatigue Damage Using Debris Particle Distributions", *Proc. 60th American Helicopter Society Annual Forum* (Baltimore, MD) June 2004 (*NASA TM-2004-212883* and Army Research Laboratory Report *ARL-TR-3133*).
- <sup>57</sup> H.J. Decker, D.G. Lewicki, and J.J. Zakrajsek, "Health Monitoring of Helicopter Input Pinion Crack Propagation Tests", *Proc. 17th International Congress and Exhibition on Condition Monitoring and Diagnostic Engineering Mgmt* (Cambridge, England) August 2004.
- <sup>58</sup> P.J. Dempsey, D.G. Lewicki, and H.J. Decker, "Transmission Bearing Damage Detection Using Decision Fusion Analysis", *NASA TM-2004-213382* and Army Research Laboratory Report *ARL-TR-3328* (Nov. 2004).
- <sup>59</sup> P.J. Dempsey, D.G. Lewicki, and D.D. Le, "Investigation of Current Methods to Identify Helicopter Gear Health," *NASA/TM-2007-214664* (NASA/Glenn Research Center, Cleveland, Ohio) 2007.
- <sup>60</sup> D.G. Lewicki and J.J. Coy, "Vibration Characteristics of OH-58A Helicopter Main Rotor Transmission," *NASA-TP-2705, AVSCOM TR 86-C-42* (April 1987).
- <sup>61</sup> C. Letellier, J. Maquet, L. Le Sceller, G. Gouesbet, and L. A. Aguirre, *J. Phys. A.* **31**, 7913 – 7927 (1998); C. Letellier and L.A. Aguirre, *Chaos* **12**, 549 (2002).







**Figure 1.** US Army's OH-58C helicopter.

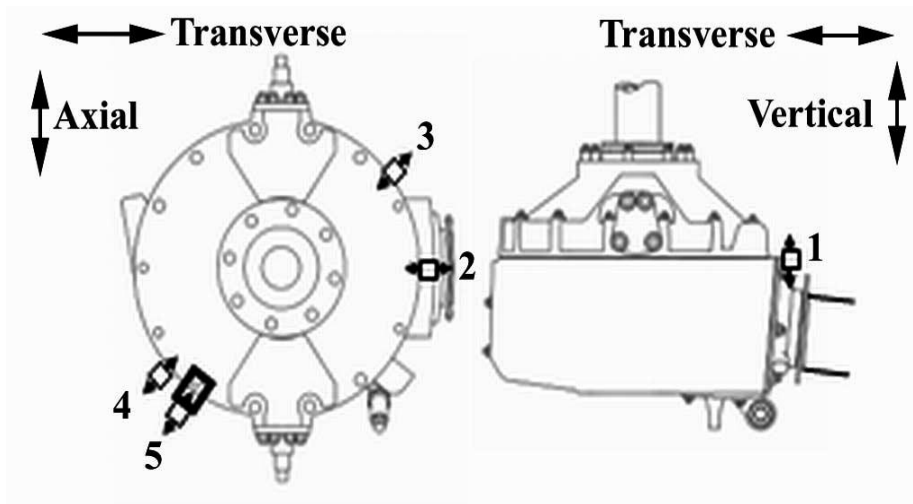
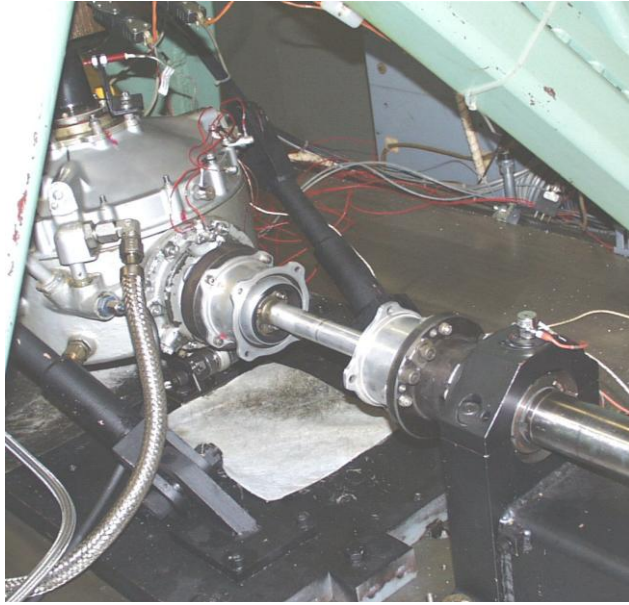
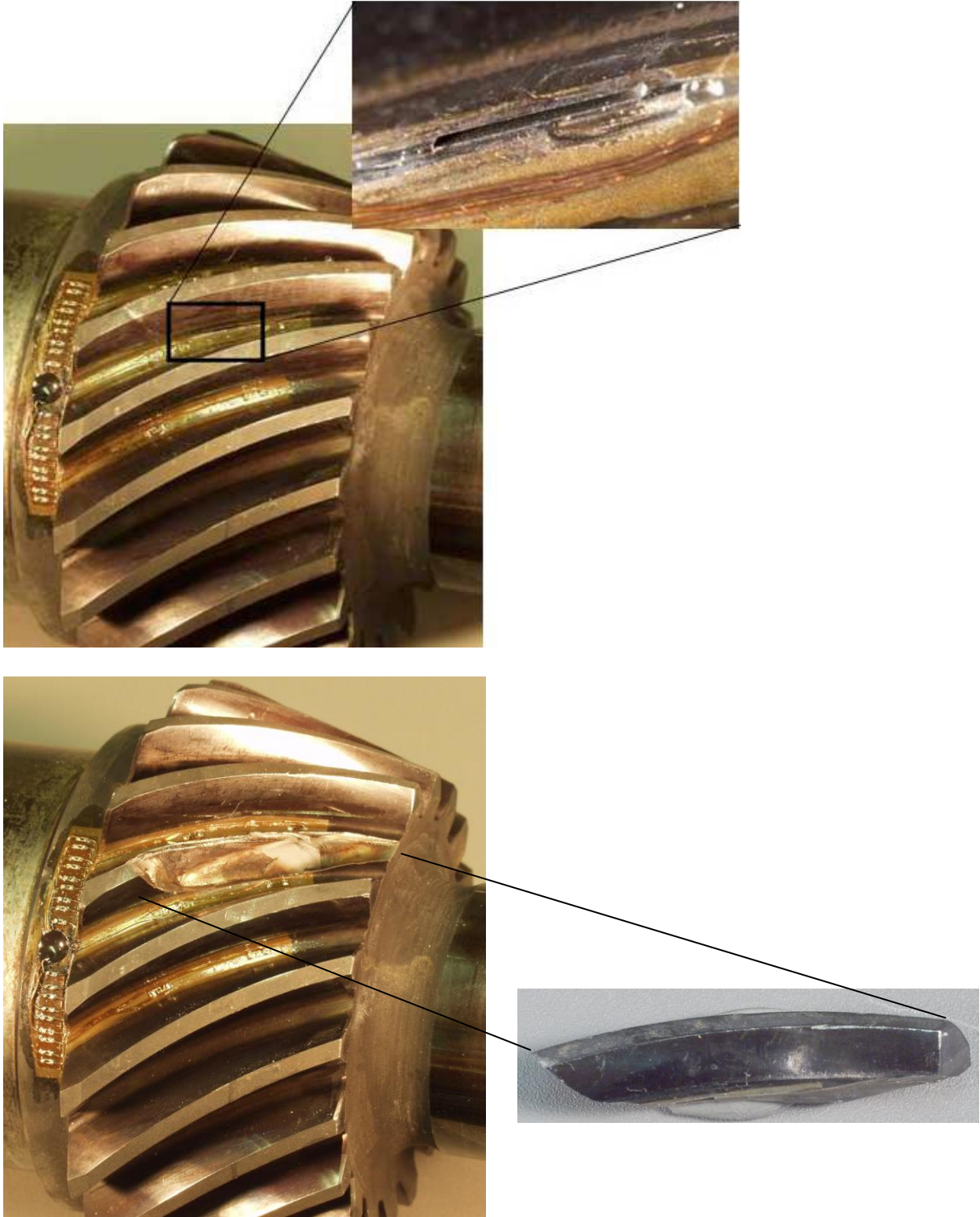
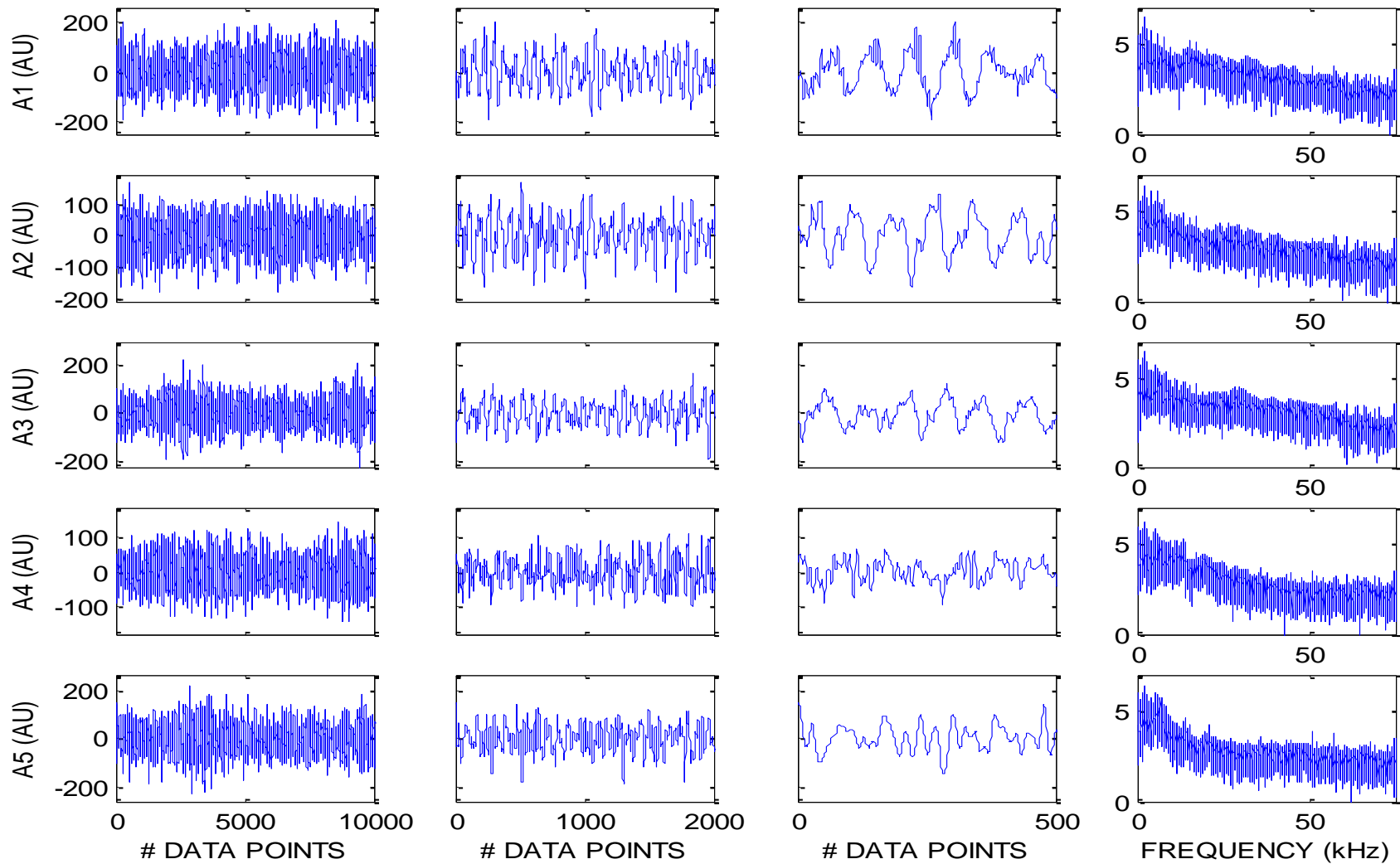


Figure 2. Pictures of the OH-58C gearbox<sup>53-54</sup> (top), and a line drawing of the accelerometer locations on the gearbox housing as viewed from the top (bottom left diagram) and side (bottom right diagram). Numbered boxes indicate the five accelerometer locations (A1 – A5), from which data were acquired during the failure testing. A1 (second channel in the original data files) was at the input side of gearbox housing to detect acceleration in the vertical (Z) direction. A2 (third channel in the original data files) was co-located with A1 to detect acceleration in the transverse (X) direction. A3 (fourth channel in the original data files) and A4 (fifth channel in the original data files) were mounted on the gearbox circumference at 45° and 225° from the input pinion gear to detect axial-traverse (X-Y) motion. A5 (sixth channel in the original data files) was on the top cover stud bracket to detect acceleration near the 225° axial-traverse direction. The accelerometers are linear to 20 kHz and have a resonance frequency of 90 kHz.



**Figure 3.** (top) Spiral-bevel pinion gear from OH-58C helicopter before removal of the broken tooth with the insert showing the seeded fault, namely an electro-discharge machined notch (3 mm wide by 0.25 mm tall by 2 mm deep); (bottom) same gear after removal of the broken tooth (insert).





**Figure 4.** Typical data from the OH-58C helicopter gearbox experiment, showing the five different accelerometer channels (A1 – A5) in each row, and over three time scales that decrease from left to right to display the underlying complex, nonlinear dynamical structure. The right-most column shows the  $\log_{10}$  of the Fourier amplitude of each signal, displaying a broad tail with no dominant frequencies.

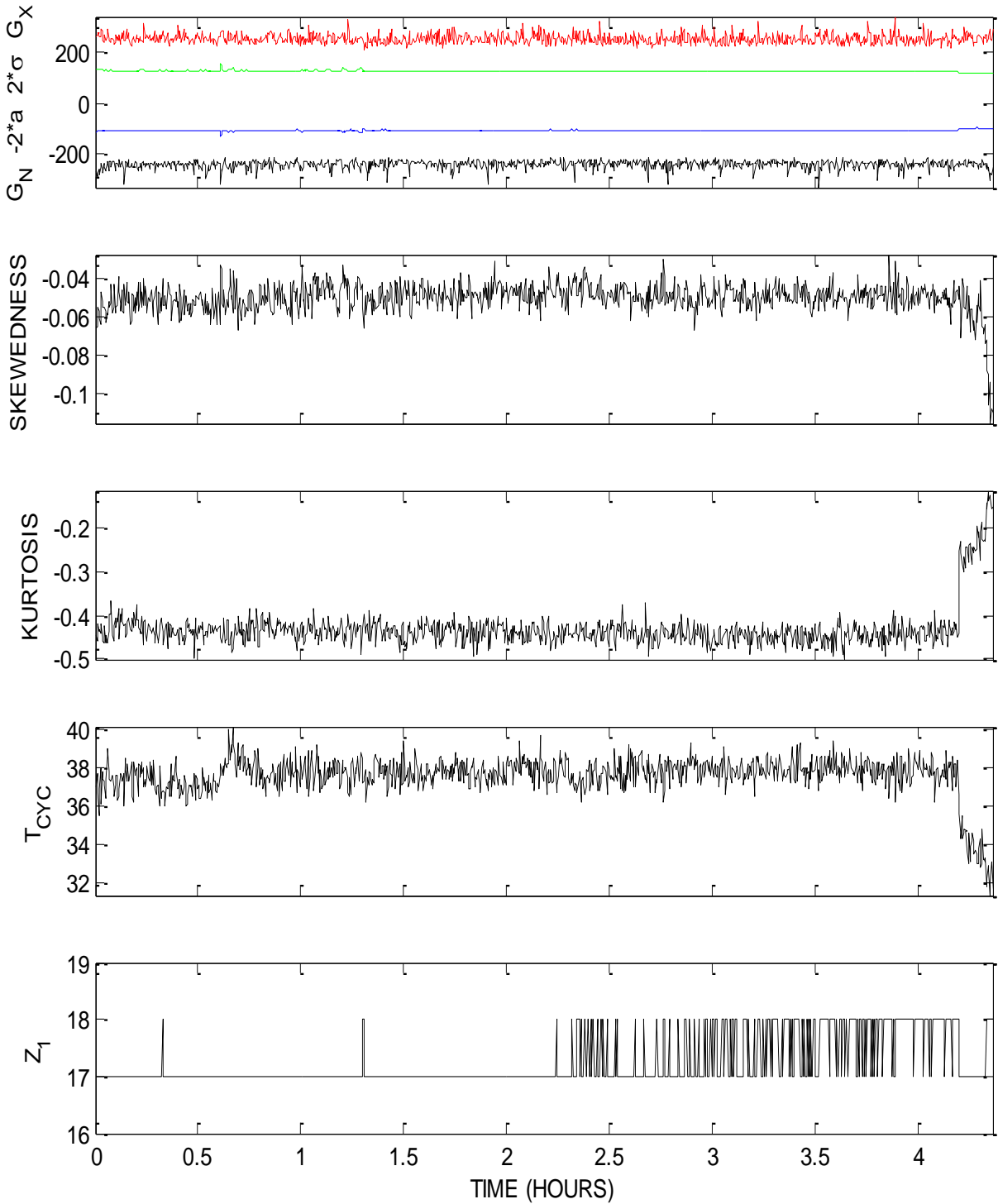


**Figure 5. Typical measures of data from the OH-58C helicopter gearbox experiment for the first accelerometer channel (A1).** The top subplot shows simple linear measures of the data, namely minimum ( $G_n$ ) in black, absolute average deviation ( $-2a$ ) in blue, standard deviation ( $2\sigma$ ) in green, and maximum ( $G_x$ ) in red. The second from the top shows skewness. The third plot from the top shows kurtosis. The second plot from the bottom shows the number of time steps per cycle ( $T_{CYC}$ ). The bottom plot shows the number of time steps to reach the first zero in the auto-correlation function ( $Z_1$ ). See the text for further discussion.

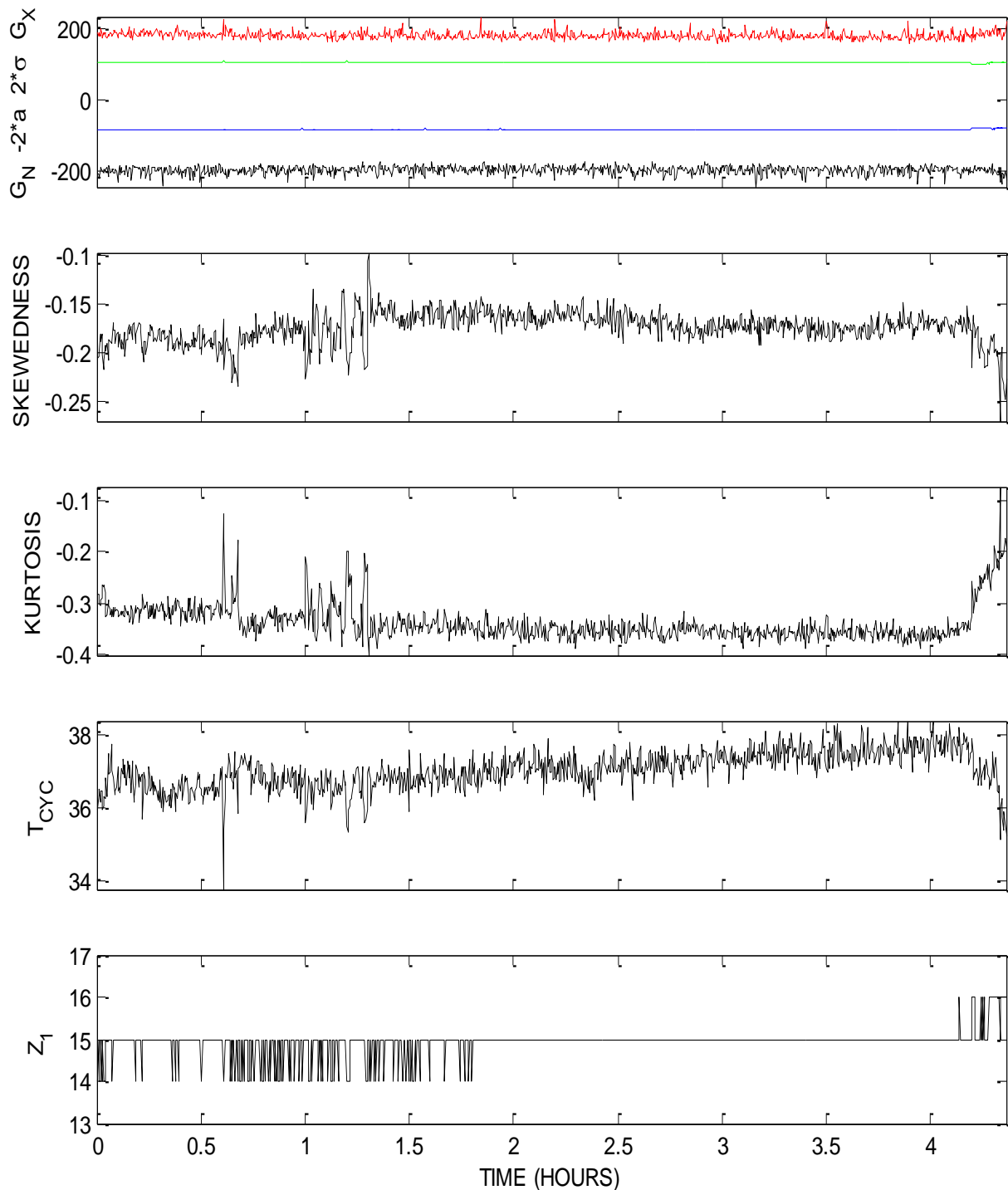


**Figure 6.** Typical measures of data from the OH-58C helicopter gearbox experiment for the second accelerometer channel (A2). The top subplot shows simple linear measures of the data, namely minimum ( $G_N$ ) in black, absolute average deviation ( $-2a$ ) in blue, standard deviation ( $2\sigma$ ) in green, and maximum ( $G_X$ ) in red. The second from the top shows skewness. The third plot from the top shows kurtosis. The second plot from the bottom shows the number of time steps per cycle ( $T_{CYC}$ ). The bottom plot shows the number of time steps to reach the first zero in the auto-correlation function ( $Z_1$ ). See the text for further discussion.

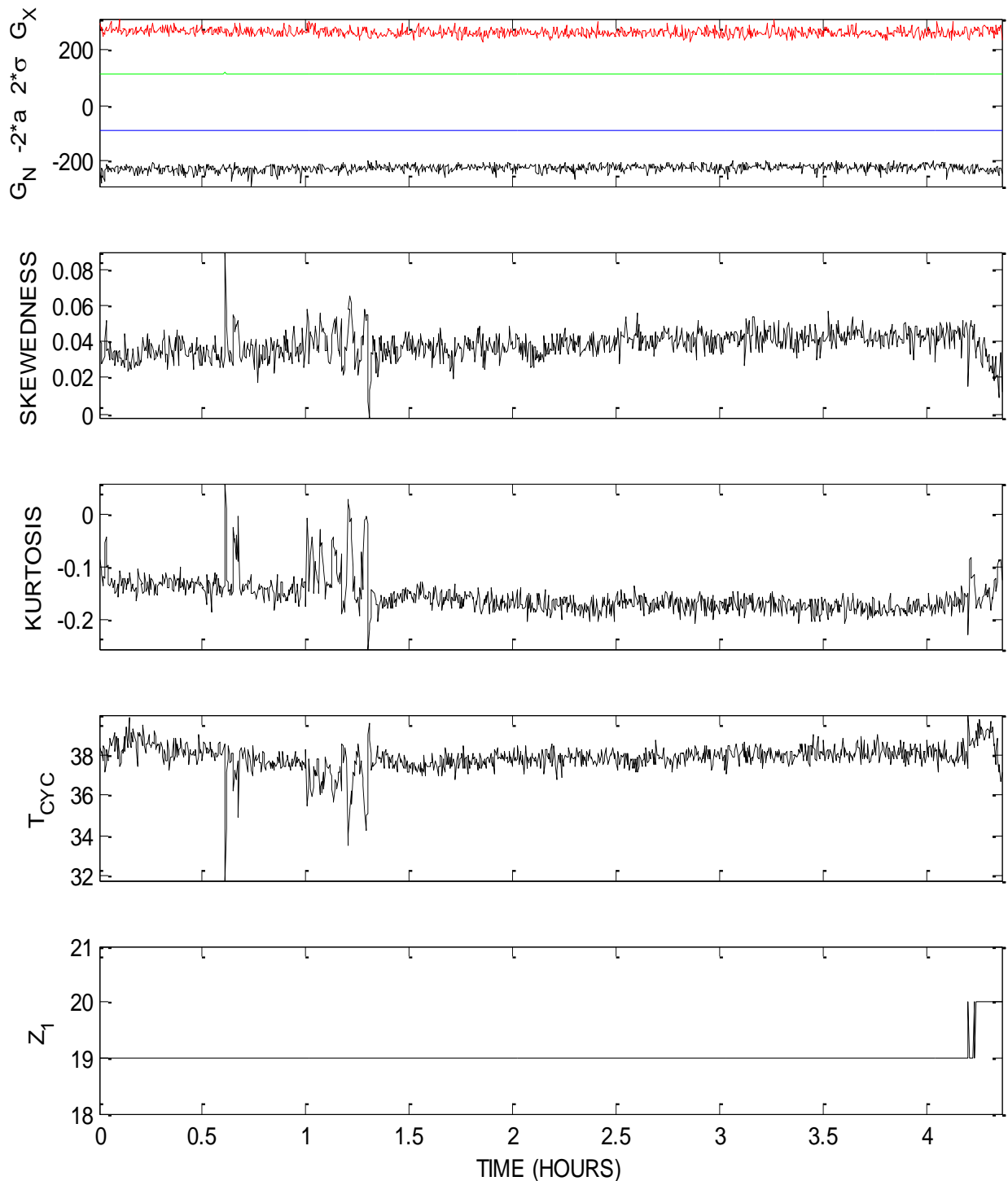


**Figure 7. Typical measures of data from the OH-58C helicopter gearbox experiment for the third accelerometer channel (A3).** The top subplot shows simple linear measures of the data, namely minimum ( $G_n$ ) in black, absolute average deviation ( $-2a$ ) in blue, standard deviation ( $2\sigma$ ) in green, and maximum ( $G_x$ ) in red. The second from the top shows skewness. The third plot from the top shows kurtosis. The second plot from the bottom shows the number of time steps per cycle ( $T_{CYC}$ ). The bottom plot shows the number of time steps to reach the first zero in the auto-correlation function ( $Z_1$ ). See the text for further discussion.

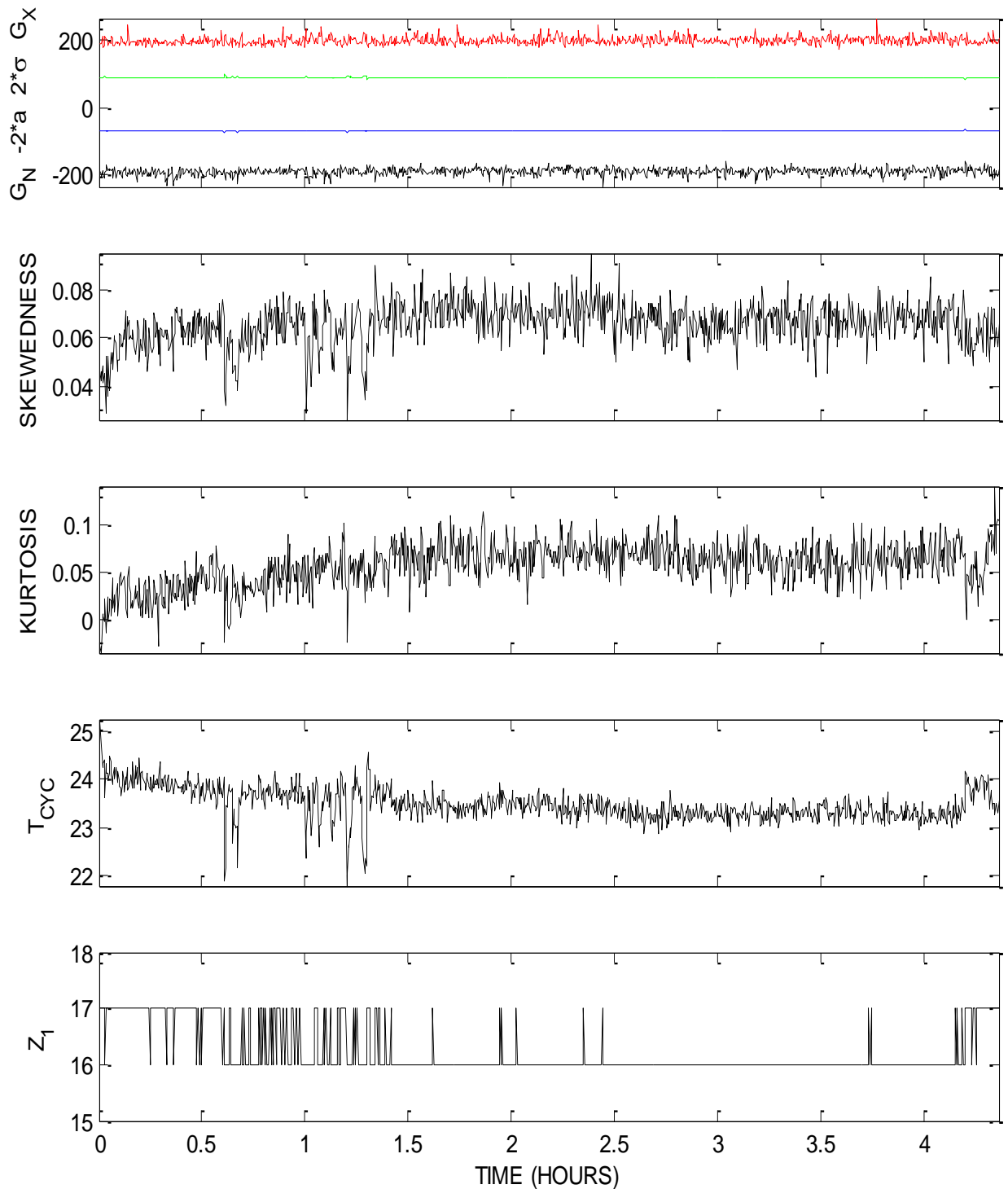


**Figure 8. Typical measures of data from the OH-58C helicopter gearbox experiment for the fourth accelerometer channel (A4).** The top subplot shows simple linear measures of the data, namely minimum ( $G_n$ ) in black, absolute average deviation ( $-2a$ ) in blue, standard deviation ( $2\sigma$ ) in green, and maximum ( $G_x$ ) in red. The second from the top shows skewness. The third plot from the top shows kurtosis. The second plot from the bottom shows the number of time steps per cycle ( $T_{CYC}$ ). The bottom plot shows the number of time steps to reach the first zero in the auto-correlation function ( $Z_1$ ). See the text for further discussion.

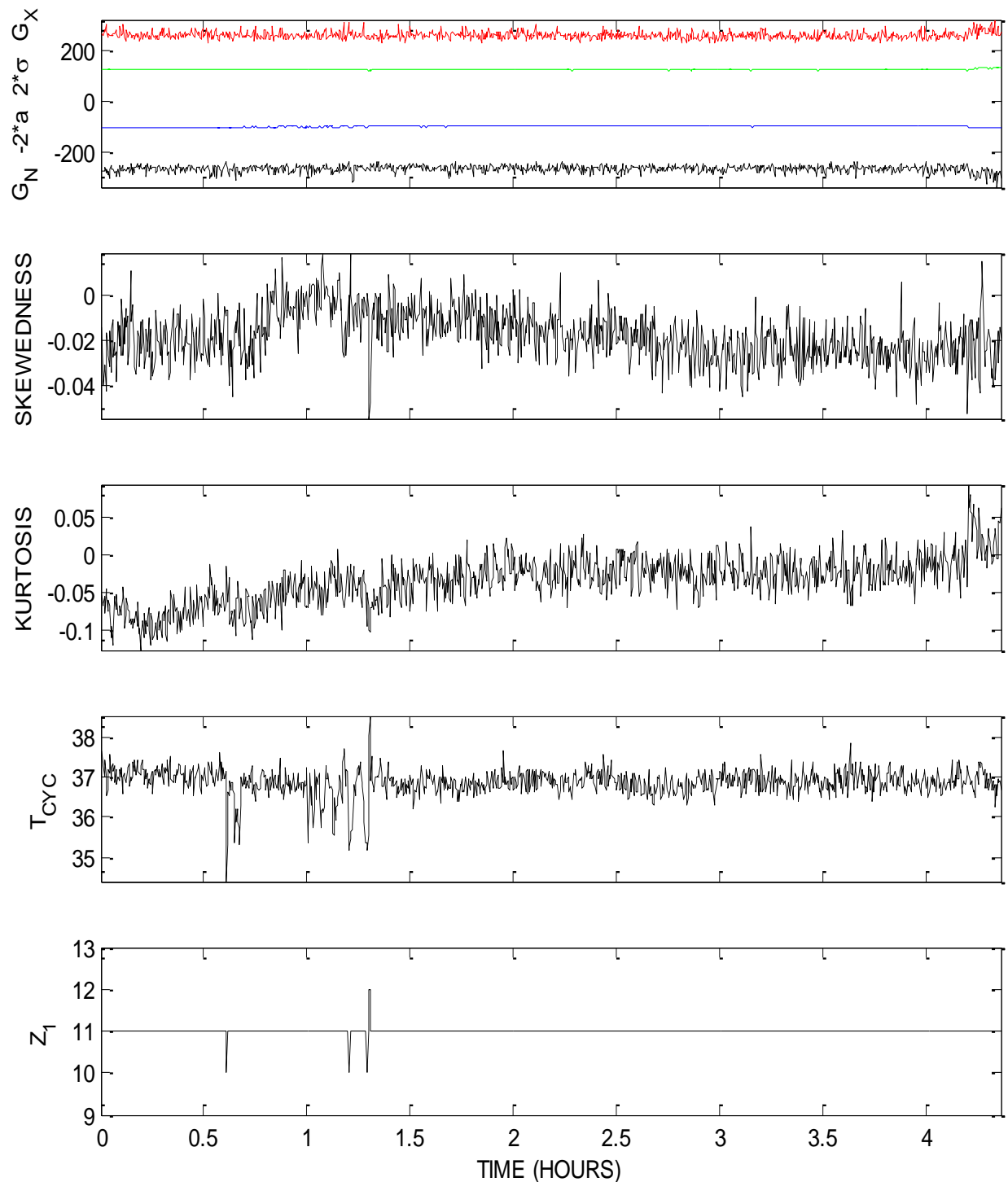


**Figure 9. Typical measures of data from the OH-58C helicopter gearbox experiment for the first accelerometer channel (A5).** The top subplot shows simple linear measures of the data, namely minimum ( $G_n$ ) in black, absolute average deviation ( $-2a$ ) in blue, standard deviation ( $2\sigma$ ) in green, and maximum ( $G_x$ ) in red. The second from the top shows skewness. The third plot from the top shows kurtosis. The second plot from the bottom shows the number of time steps per cycle ( $T_{CYC}$ ). The bottom plot shows the number of time steps to reach the first zero in the auto-correlation function ( $Z_1$ ). See the text for further discussion.

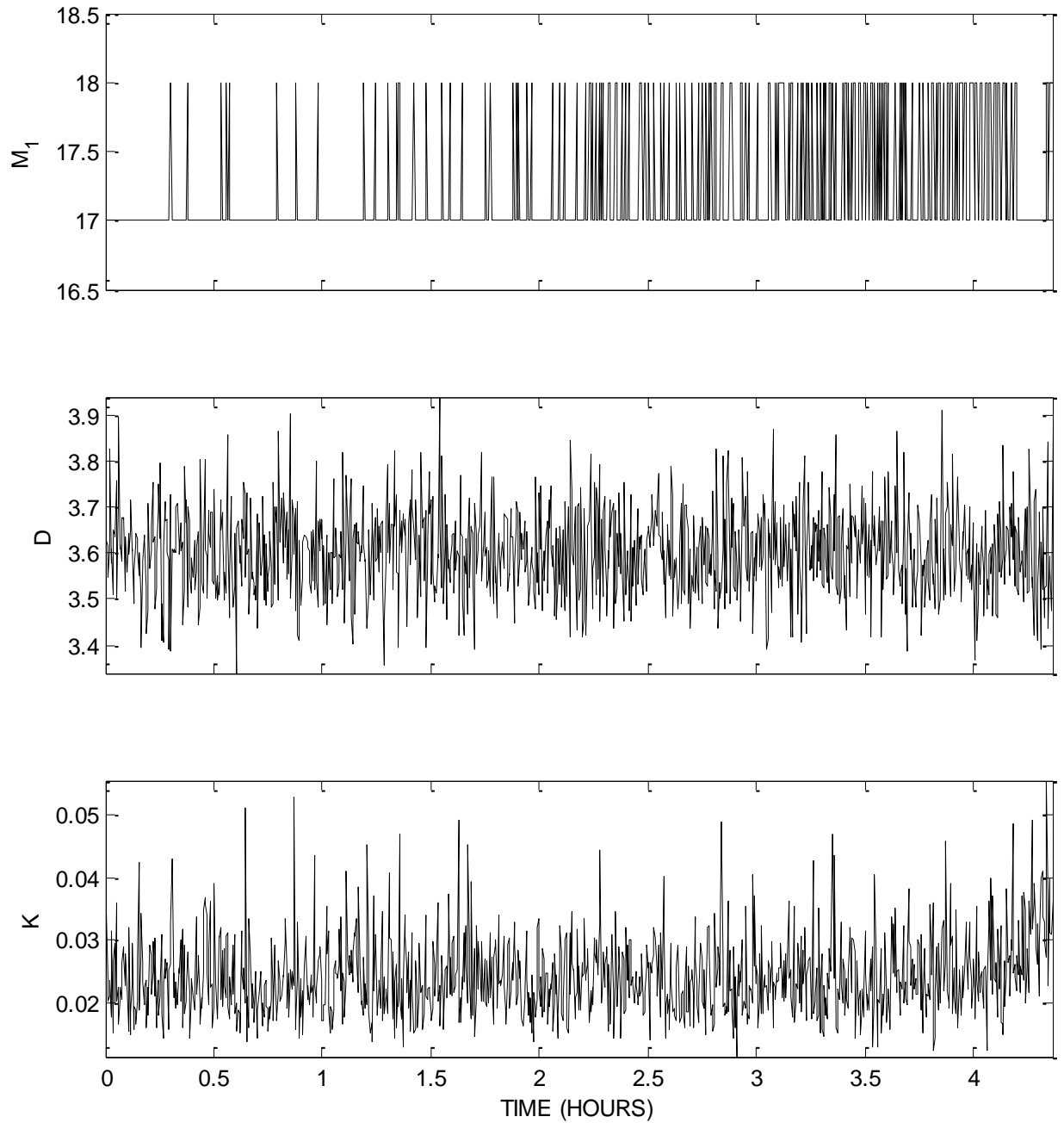


**Figure 10. Traditional nonlinear measures of the first accelerometer channel (A1) from the OH-58C helicopter gearbox experiment.** The top subplot shows the number of time steps to reach the first minimum in the mutual information function ( $M_1$ ). The middle plot displays the correlation dimension ( $D$ ), as a measure of complexity in the data. The bottom plot shows the Kolmogorov entropy ( $K$ ), which measures the loss in predictability (bits per second). See the text for further discussion.

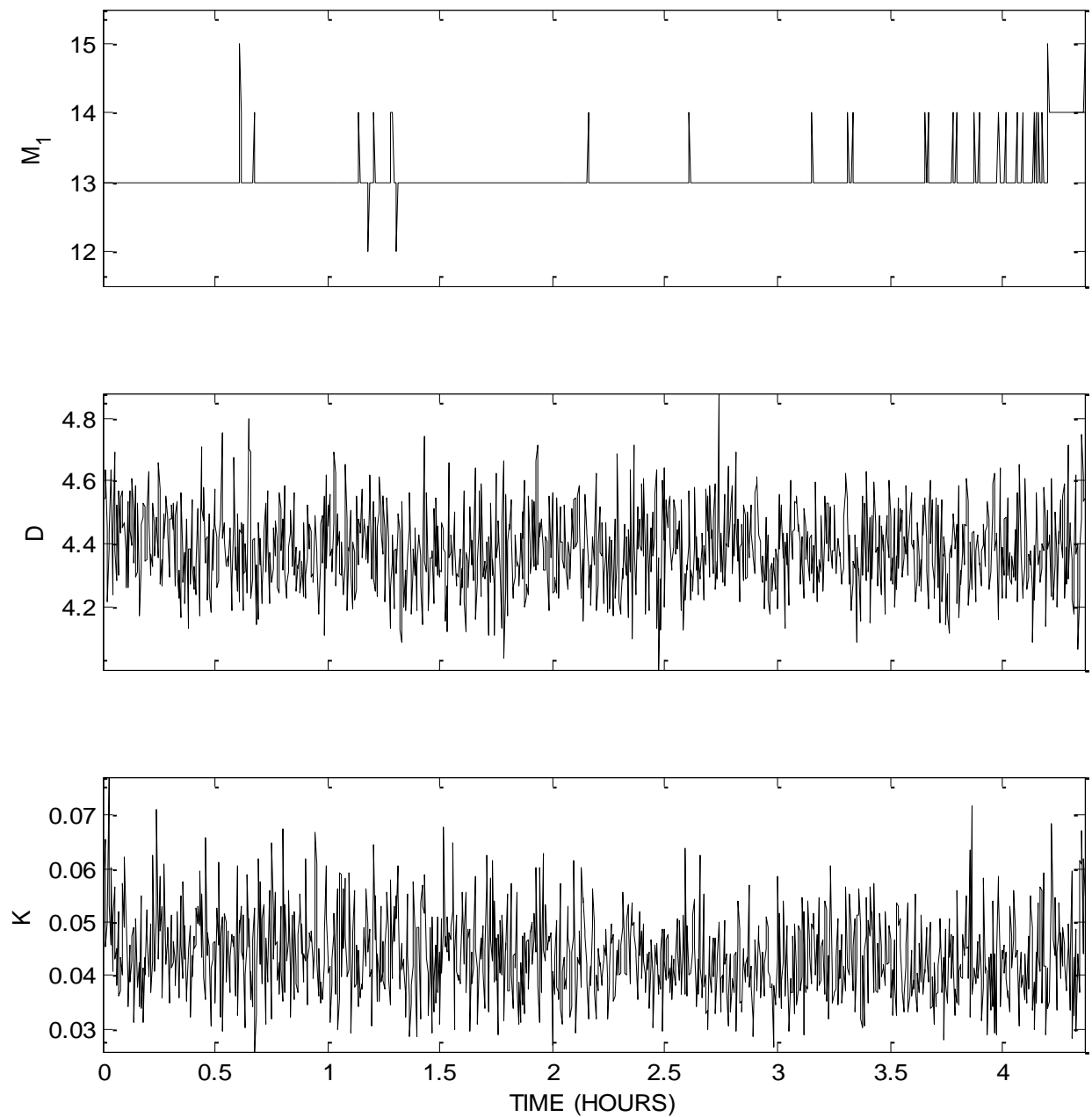


**Figure 11. Traditional nonlinear measures of the second accelerometer channel (A2) from the OH-58C helicopter gearbox experiment.** The top subplot shows the number of time steps to reach the first minimum in the mutual information function ( $M_1$ ). The middle plot displays the correlation dimension ( $D$ ), as a measure of complexity in the data. The bottom plot shows the Kolmogorov entropy ( $K$ ), which measures the loss in predictability (bits per second). See the text for further discussion.

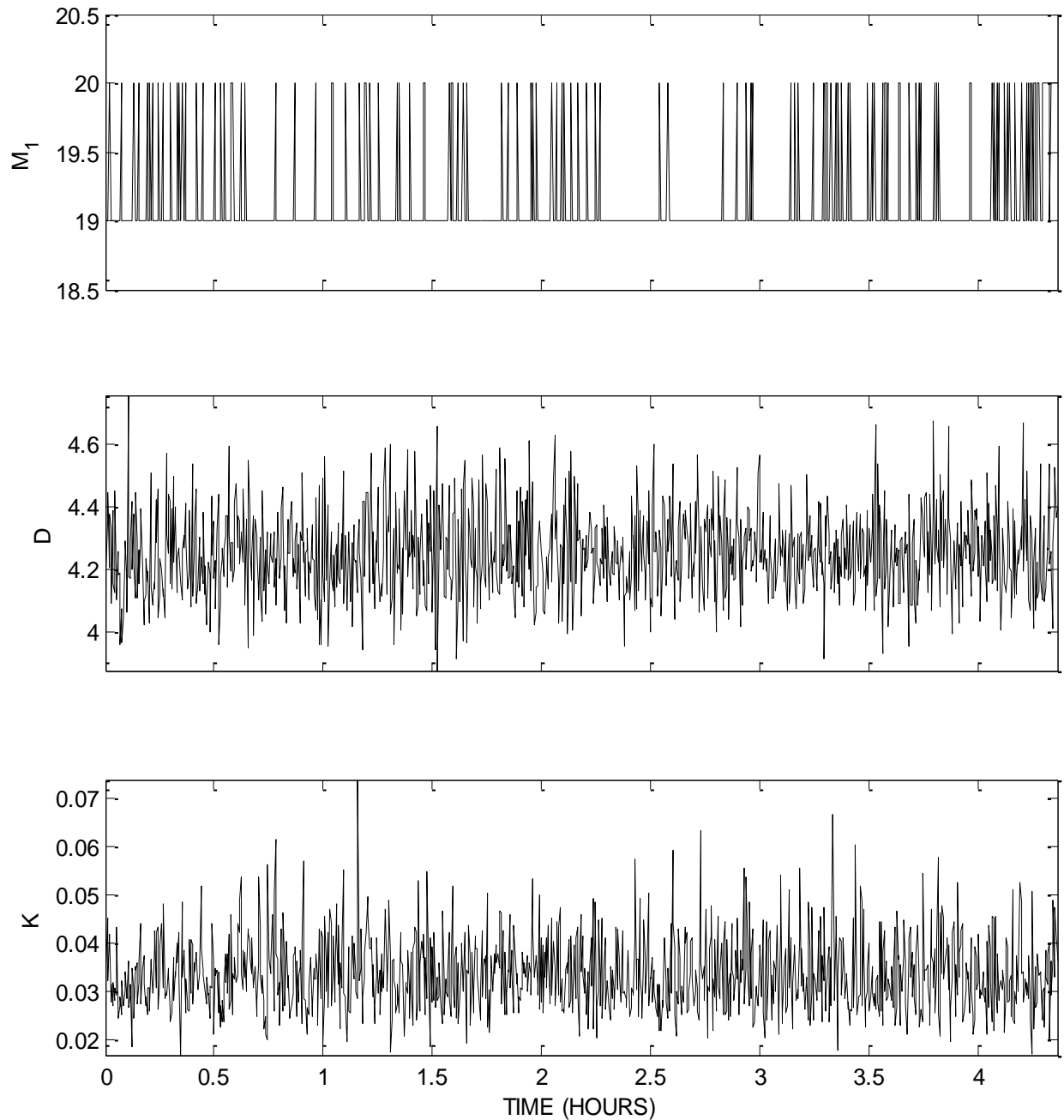


**Figure 12. Traditional nonlinear measures of the third channel (A3) from the OH-58C helicopter gearbox experiment.** The top subplot shows the number of time steps to reach the first minimum in the mutual information function ( $M_1$ ). The middle plot displays the correlation dimension ( $D$ ), as a measure of complexity in the data. The bottom plot shows the Kolmogorov entropy ( $K$ ), which measures the loss in predictability (bits per second). See the text for further discussion.

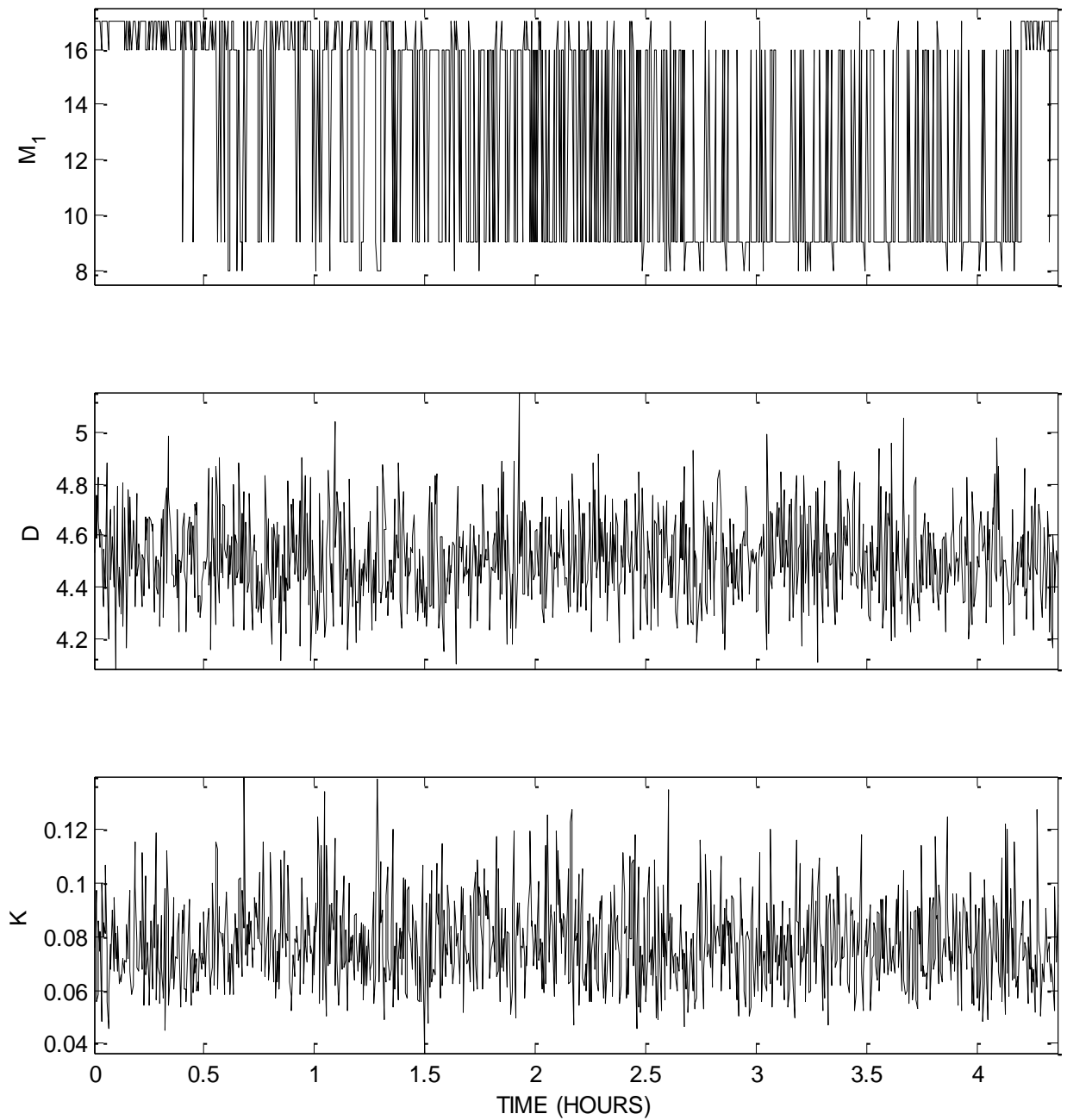


**Figure 13. Traditional nonlinear measures of the fourth accelerometer channel (A4) from the OH-58C helicopter gearbox experiment.** The top subplot shows the number of time steps to reach the first minimum in the mutual information function ( $M_1$ ). The middle plot displays the correlation dimension ( $D$ ), as a measure of complexity in the data. The bottom plot shows the Kolmogorov entropy ( $K$ ), which measures the loss in predictability (bits per second). See the text for further discussion.

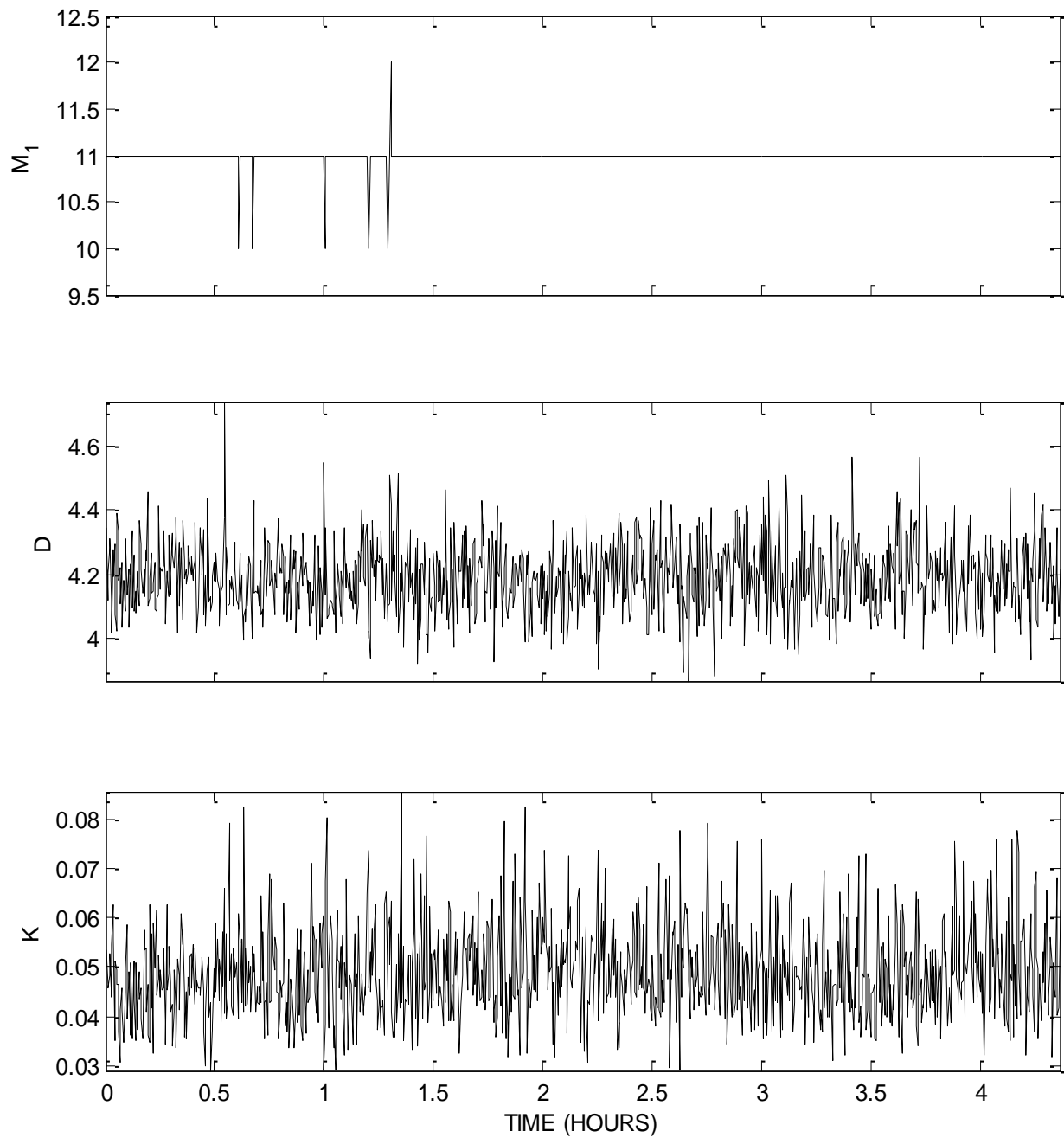


**Figure 14. Traditional nonlinear measures of the fifth accelerometer channel (A5) from the OH-58C helicopter gearbox experiment.** The top subplot shows the number of time steps to reach the first minimum in the mutual information function ( $M_1$ ). The middle plot displays the correlation dimension ( $D$ ), as a measure of complexity in the data. The bottom plot shows the Kolmogorov entropy ( $K$ ), which measures the loss in predictability (bits per second). See the text for further discussion.

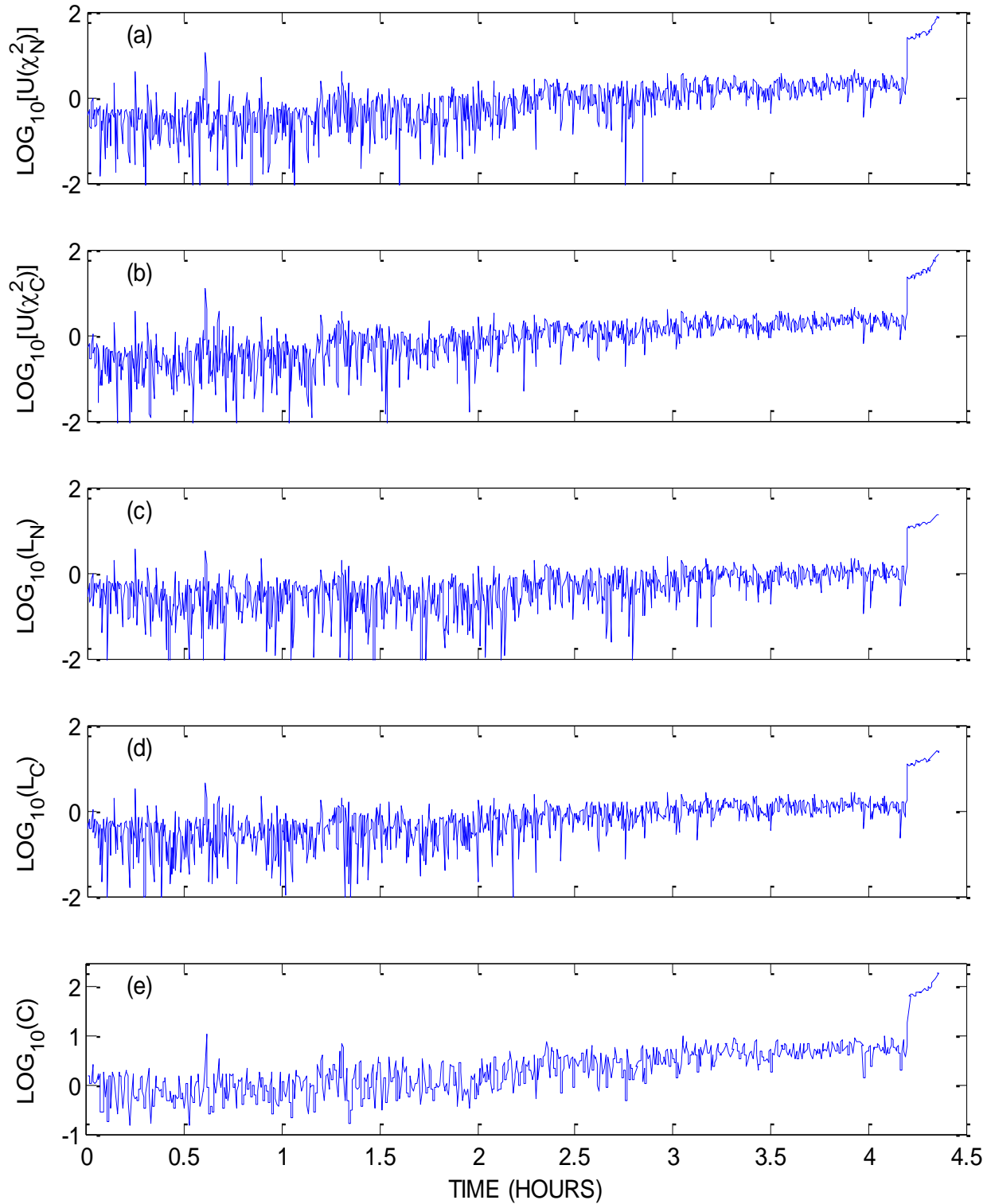


**Figure 15.** Phase-space dissimilarity measures versus time for accelerometer channel, A1 with  $S=2$ ,  $d=3$ ,  $\lambda=18$ : (a) normalized  $\chi^2$  measure for the non-connected phase-space,  $U(\chi_N^2)$ ; (b) normalized  $\chi^2$  measure for the connected phase-space,  $U(\chi_C^2)$ ; (c) normalized  $L_1$  measure for the non-connected phase-space,  $U(L_N)$ ; (d) normalized  $L_1$  measure for the connected phase-space,  $U(L_C)$ ; (e) composite measure,  $C$ .

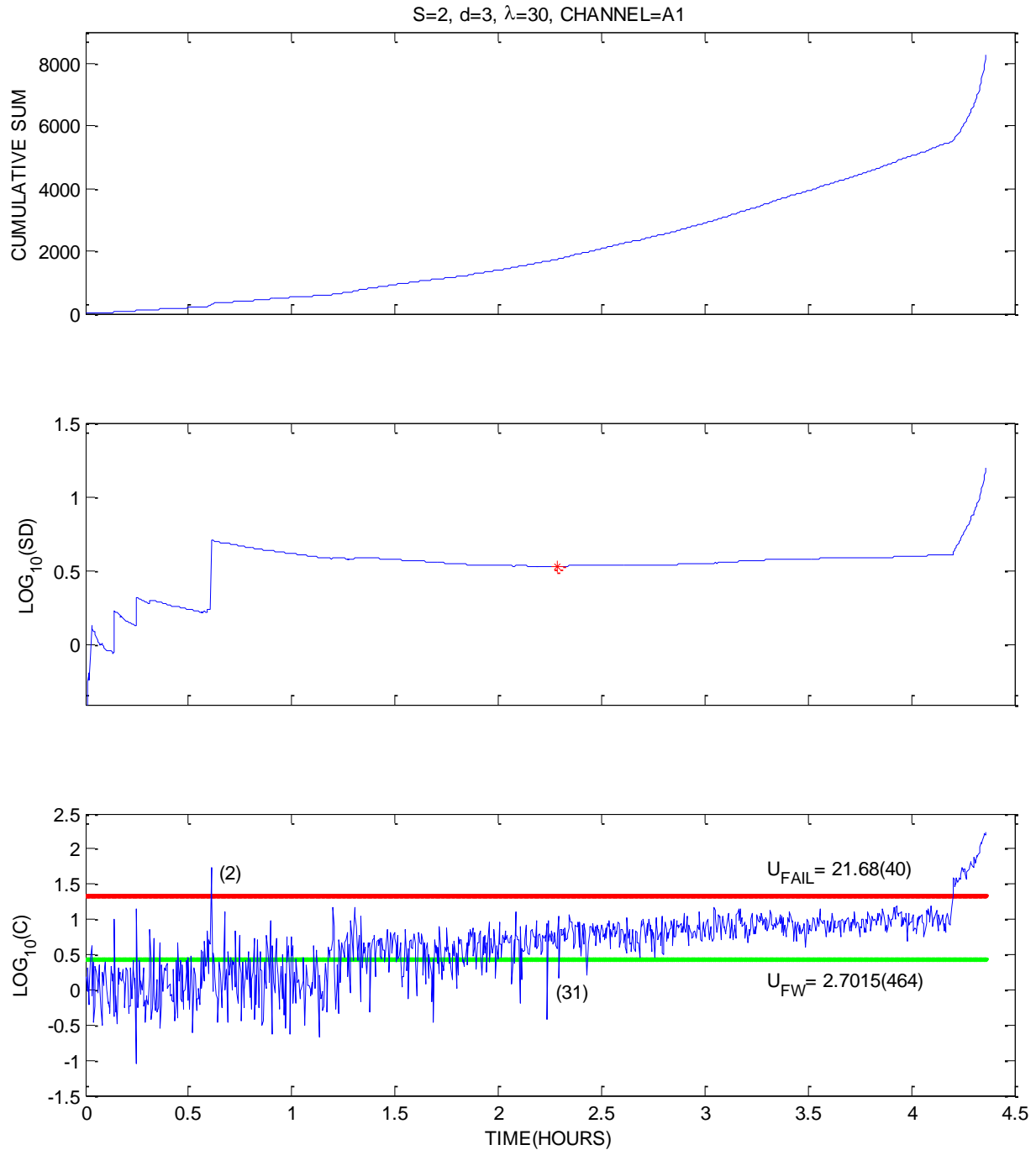


**Figure 16.** Best forewarning of gear failure via the composite phase-space dissimilarity measure for accelerometer channel, A1, at  $S=2$ ,  $d=3$ ,  $\lambda=30$  showing: (top) the cumulative sum over time; (middle) the standard deviation (SD) from a linear fit versus time, with a star (\*) at the corresponding minimum; and (bottom) the composite PSDM versus time with a threshold for forewarning (green) and another threshold for failure onset (red).

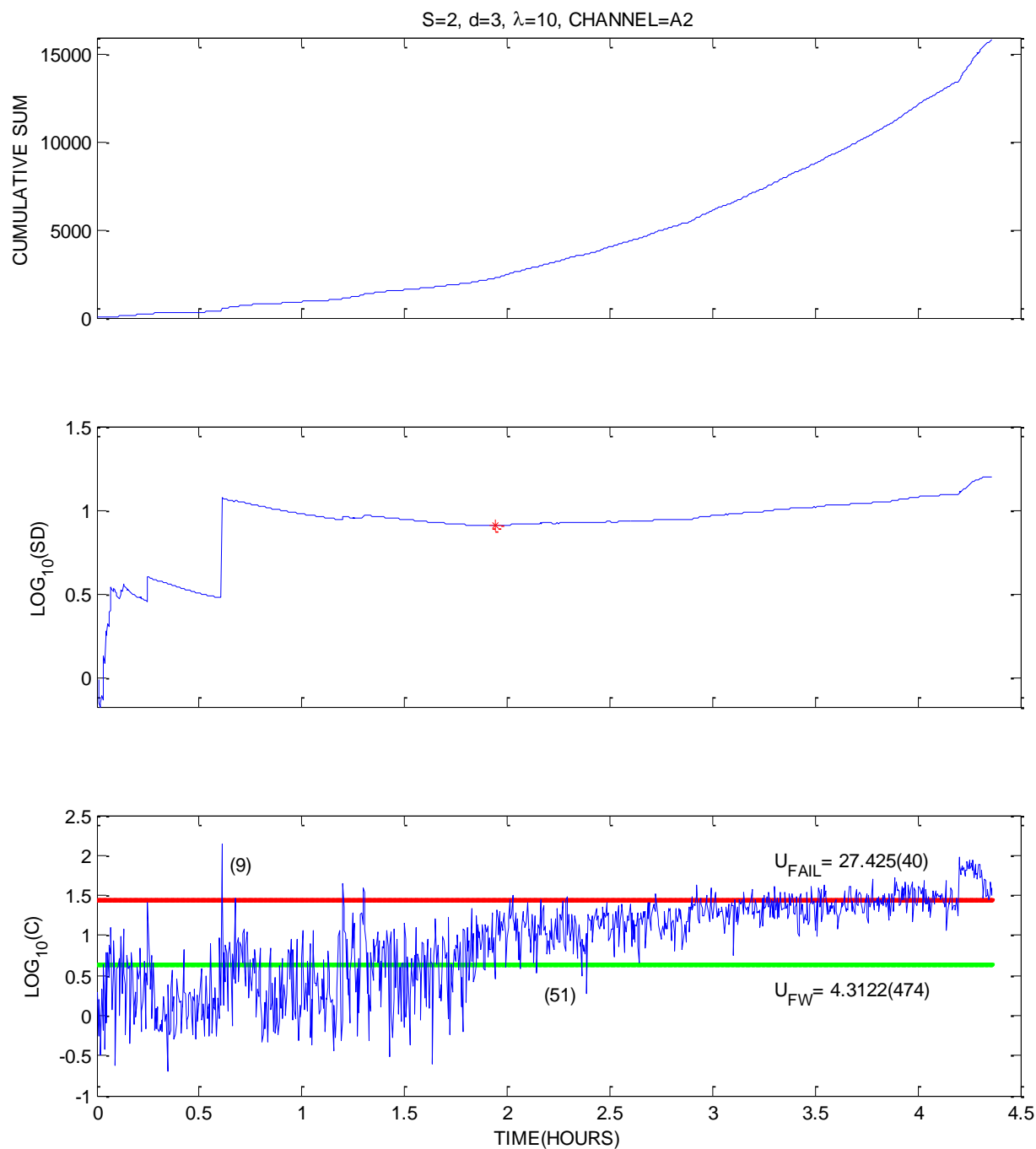


**Figure 17.** Best forewarning of gear failure via the composite phase-space dissimilarity measure for accelerometer channel, A2, at  $S=2$ ,  $d=3$ ,  $\lambda=10$  showing: (top) the cumulative sum over time; (middle) the standard deviation (SD) from a linear fit versus time, with a star (\*) at the corresponding minimum; and (bottom) the composite PSDM versus time with a threshold for forewarning (green) and another threshold for failure onset (red).

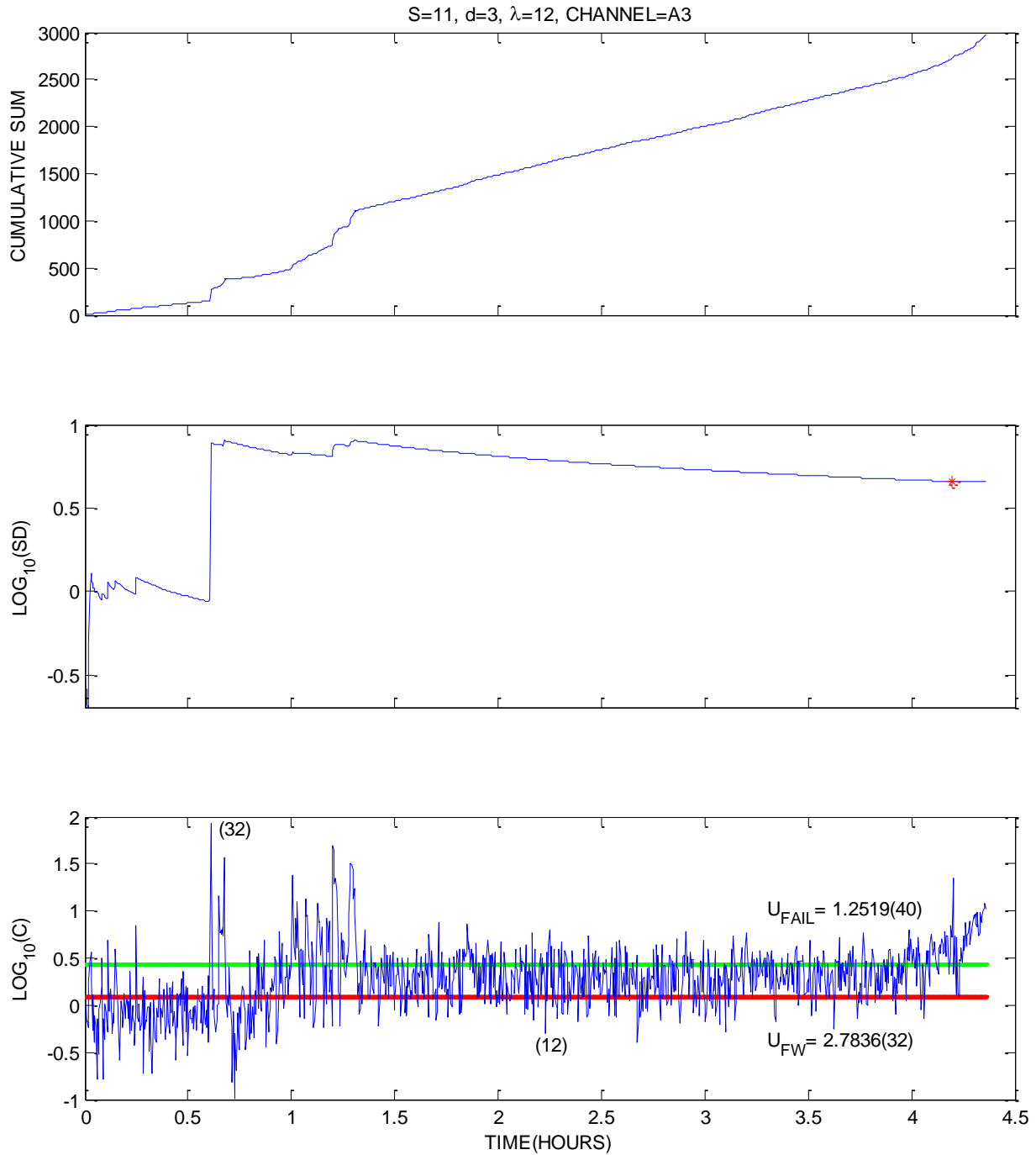


**Figure 18.** Best forewarning of gear failure via the composite phase-space dissimilarity measure for accelerometer channel, A3, at  $S=11$ ,  $d=3$ ,  $\lambda=12$  showing: (top) the cumulative sum over time; (middle) the standard deviation (SD) from a linear fit versus time, with a star (\*) at the corresponding minimum; and (bottom) the composite PSDM versus time with a threshold for forewarning (green) and another threshold for failure onset (red).

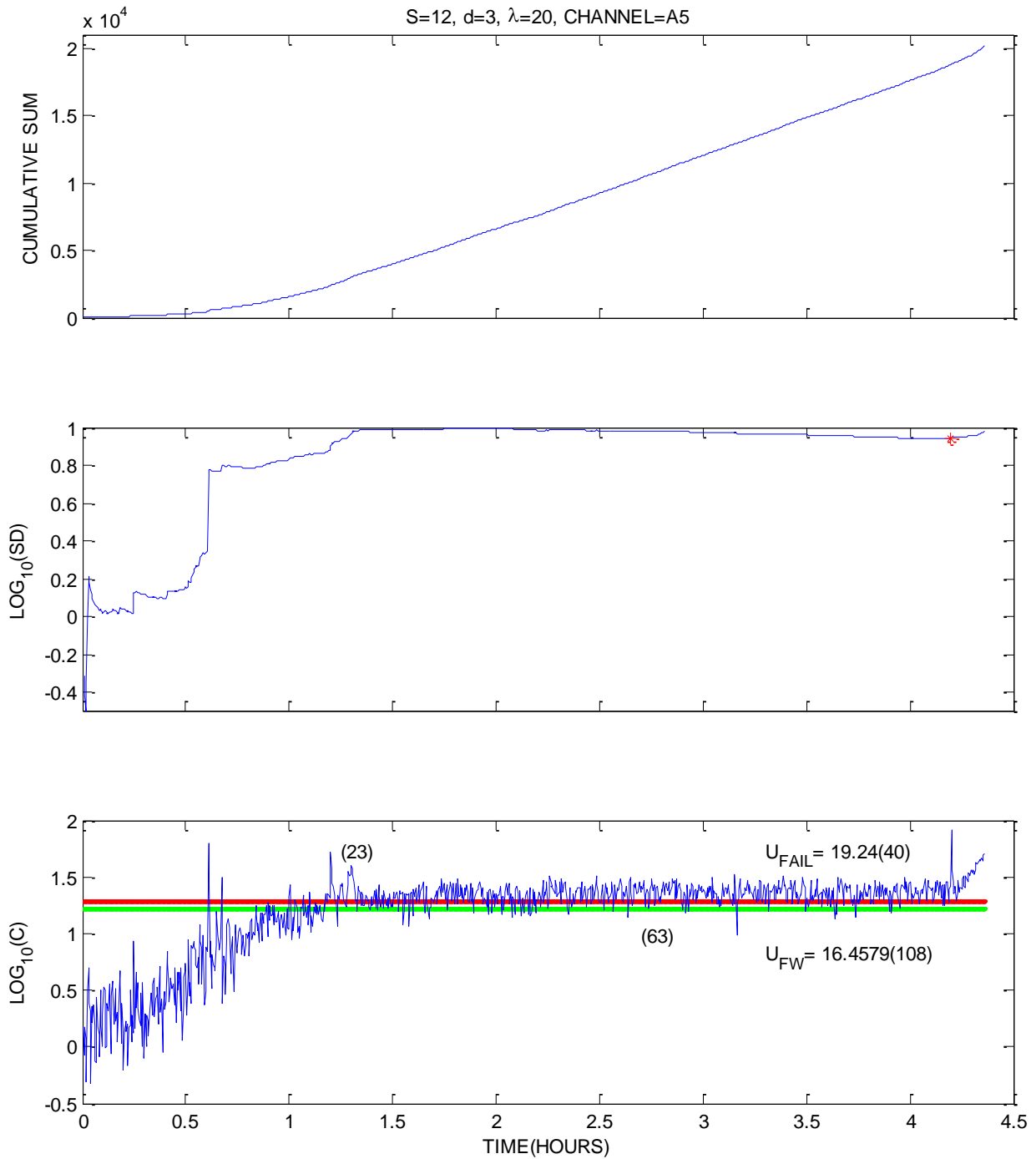


**Figure 19.** Best forewarning of gear failure via the composite phase-space dissimilarity measure for accelerometer channel, A5, at  $S=12$ ,  $d=3$ ,  $\lambda=20$  showing: (top) the cumulative sum over time; (middle) the standard deviation (SD) from a linear fit versus time, with a star (\*) at the corresponding minimum; and (bottom) the composite PSDM versus time with a threshold for forewarning (green) and another threshold for failure onset (red).

**INTERNAL DISTRIBUTION**

1. L. M. Hively
2. J. P. Trien
3. B. A. Worley
4. A. S. Loebel
5. Central Research Library
6. ORNL Laboratory Records-RC
7. ORNL Laboratory Records-OSTI

**EXTERNAL DISTRIBUTION**

8. U.S. Army Research Laboratory, 2800 Powder Mill Road, Adelphi, Maryland, 20783-1138  
Attention: RDRL-SER-E (A. Bayba)  
Attention: RDRL-SER-M (M. Conn)  
Attention: RDRL-SER-L (L. Currano)  
Attention: RDRL-SER-E (R. Del Rosario)  
Attention: RDRL-SER-E (G. Mitchell)  
Attention: RDRL-SER-E (C. Ly)  
Attention: RDRL-SER-U (K. Ranney)  
Attention: RDRL-SER-E (K. Tom)  
Attention: RDRL-SER-E (D. Washington)
9. U.S. Army Research Laboratory VTD, NASA Glenn Research Center, 21000 Brookpark Road,  
M.S.23-3, Cleveland, Ohio, 44135  
Attention: T. Krantz  
Attention: D. Lewicki
10. Selma Matthews, Senior Research Scientist, CERDEC Command and Control Directorate,  
AMSRD-CER-C2-AP-PT, 10108 Gridley Road, Suite 1, Fort Belvoir, Virginia, 22060-5816